View metadata, citation and similar papers at core.ac.uk

brought to you by CORE

provided by Warwick Research Archives Portal Repository

Manuscript version: Author's Accepted Manuscript
The version presented in WRAP is the author's accepted manuscript and may differ from the published version or Version of Record.

Persistent WRAP URL:
http://wrap.warwick.ac.uk/135328

How to cite:
Please refer to published version for the most recent bibliographic citation information. If a published version is known of, the repository item page linked to above, will contain details on accessing it.

Copyright and reuse:
The Warwick Research Archive Portal (WRAP) makes this work by researchers of the University of Warwick available open access under the following conditions.

Copyright © and all moral rights to the version of the paper presented here belong to the individual author(s) and/or other copyright owners. To the extent reasonable and practicable the material made available in WRAP has been checked for eligibility before being made available.

Copies of full items can be used for personal research or study, educational, or not-for-profit purposes without prior permission or charge. Provided that the authors, title and full bibliographic details are credited, a hyperlink and/or URL is given for the original metadata page and the content is not changed in any way.

Publisher's statement:
Please refer to the repository item page, publisher's statement section, for further information.

For more information, please contact the WRAP Team at: wrap@warwick.ac.uk.

warwick.ac.uk/lib-publications

Relaying Systems With Reciprocity Mismatch: Impact Analysis and Calibration

Rongjiang Nie, Li Chen, Nan Zhao, *Senior Member, IEEE*,
Yunfei Chen, *Senior Member, IEEE*, F. Richard Yu, *Fellow, IEEE*, and Guo Wei

***Abstract*—Cooperative beamforming can provide significant performance improvement for relaying systems with the help of the channel state information (CSI). In time-division duplexing (TDD) mode, the estimated CSI will deteriorate due to the reciprocity mismatch. In this work, we examine the impact and the calibration of the reciprocity mismatch in relaying systems. To evaluate the impact of the reciprocity mismatch for all devices, the closed-form expression of the achievable rate is first derived. Then, we analyze the performance loss caused by the reciprocity mismatch at sources, relays, and destinations respectively to show that the mismatch at relays dominates the impact. To compensate the performance loss, a two-stage calibration scheme is proposed for relays. Specifically, relays perform the intra-calibration based on circuits independently. Further, the inter-calibration based on the discrete Fourier transform (DFT) codebook is operated to improve the calibration performance by cooperation transmission, which has never been considered in previous work. Finally, we derive the achievable rate after relays perform the proposed reciprocity calibration scheme and investigate the impact of estimation errors on the system performance. Simulation results are presented to verify the analytical results and to show the performance of the proposed calibration approach.**

***Index Terms*—Cooperative beamforming, reciprocity calibration, reciprocity mismatch, time-division duplexing.**

I. Introduction

Relaying is an advanced technique for wireless networks to improve the system performance significantly, and has been widely studied in vehicular networks, cognitive radio networks and ad hoc networks [1]–[3]. A typical relaying system contains multiple source-destination (S-D) pairs and multiple relays. The relays support the communications of the S-D pairs by cooperative beamforming with the knowledge of channel state information (CSI) [4]–[6].

Generally, CSI is estimated from training pilots in the time division duplexing (TDD) mode, which will result in reciprocity mismatch of downlink and uplink CSI. This is because the overall channel consists of not only the wireless propagation channel, but also the radio frequency (RF) gains due to the frequency responses of hardwares [7], e.g., analog-to-digital converters (ADC), digital-to-analog converters (DAC), filters and amplifiers. Although uplink and downlink wireless propagation channels may be reciprocal, the radio frequency (RF) gains of different hardwares are asymmetric, which causes the reciprocity mismatch [8].

To investigate the impact of the reciprocity mismatch on system performance, previous works have provided theoretical analyses [9]–[12] and experimental results [13], [14]. The reciprocity mismatch at base station (BS) seriously degrades the performance of multiple-input multiple-output (MIMO) system with linear beamforming approaches such as zero-forcing (ZF) and matched filter (MF). The comparison between the performance of the two beamforming methods indicates that ZF outperforms MF [9]. But ZF is also more sensitive to the reciprocity mismatch than MF, especially in the high signal-to-noise ratio (SNR) regime [10]. In massive MIMO, ZF and MF almost achieve the same performance in asymptotic comparisons [11]. It is noticed that the impact of the mismatch at user equipment (UE) side is much smaller than that at BS side [12]. Further, the experimental results in [13], [14] verified the performance loss due to the reciprocity mismatch and put forward insights on how the mismatch evolves in time and frequency domains.

Since the reciprocity mismatch has a great impact on system performance, reciprocity calibration is essential for TDD systems. Calibration approaches can be mainly divided into the hardware-circuit calibration and the signal-space calibration. In the hardware-circuit calibration, auxiliary hardwares, such as switches and couplers, are implemented to connect transmit antennas and receive antennas. In [15], an automatic hardware-circuit calibration was first presented for MIMO. Then, the hardware-circuit calibration was applied to the wideband wireless systems, where different subcarriers were independently calibrated in [16]. Unlike the hardware-circuit calibration requiring extra hardwares, the signal-space calibration only requires over-the-air signals among uncalibrated antennas. A signal-space calibration called relative calibration was first proposed to calibrate the TDD single-input single-output system in the frequency domain [17]. For multi-user MIMO, the signal-space calibration requires UEs to feed back CSI to BS and utilizes the total least-square (LS) method to estimate calibration coefficients [18]. Then, a low-complexity conjugate gradient algorithm was proposed for solving the total LS problem in [19]. For wideband MIMO, B. Kouassi *et*

This research was supported by National Key Research and Development Project under 2018YFB1801105, USTC Research Funds of the Double First-Class Initiative (Grant No. YD3500002001), and Yunfei Chen acknowledges the support of EC H2020 DAWN4IoE (778305). This paper was presented in part at the IEEE Global Conference on Signal and Information Processing (GlobalSIP), Ottawa, Canada, November 2019. (*Corresponding author: Li Chen*)

R. Nie, L. Chen and G. Wei are with Department of Electronic Engineering and Information Science, University of Science and Technology of China. (e-mail: johnnrj@mail.ustc.edu.cn, {chenli87, wei}@ustc.edu.cn).

N. Zhao is with the School of Info. and Commun. Eng., Dalian University of Technology, Dalian 116024, China. (e-mail:zhaonan@dlut.edu.cn).

Y. Chen is with the School of Engineering, University of Warwick, Coventry CV4 7AL, U.K. (e-mail: Yunfei.Chen@warwick.ac.uk).

F.R. Yu is with the Department of Systems and Computer Engineering, Carleton University, Ottawa, ON, K1S 5B6, Canada. (email: richard.yu@carleton.ca).

al. presented a time-domain reciprocity calibration, to avoid calibrating each subcarrier respectively [20].

In massive MIMO, the reciprocity calibration methods of conventional system encounter challenges due to high circuit costs or large amounts of the overhead for feeding back CSI. To reduce the costs of hardwares, a daisy chain interconnection topology of the circuits was applied to the hardware-circuit calibration in [21], which reduces transceiver interconnection effort. To avoid feeding back CSI from UEs in the signal-space calibration, a series calibration approaches called "single-side" or "one-side" calibration were presented for massive MIMO based on the results in [22]. In [23], a single-side calibration method was presented for the massive MIMO Argos prototype. The Argos calibration only calibrates the antennas of BS and does not calibrate the antennas of UEs. The performance of the Argos calibration approach is sensitive to fading channels and relies on the location of the reference antenna. To overcome the shortages, H. Wei *et al.* presented the mutual coupling calibration, which utilized the strong mutual coupling effects among adjacent antennas rather than fading channels [24]. In [25], an over-the-air calibration framework was proposed based on some existing signal-space calibration schemes which were different special cases of antenna grouping schemes in the framework. To further relieve the impact of the reciprocity mismatch at the UE side, O. Raeesi *et al.* proposed an calibration approach incorporating a dedicated round-trip pilot signaling with feasible pilot overhead for the acquisition of calibration coefficients at the BS [26].

For distributed MIMO, the reciprocity calibration is also difficult due to the long distance between BSs or access points. In [27], R. Rogalin *at el.* proposed a hierarchical calibration for distributed MIMO, which applied the LS method to estimate calibration coefficients. Then, in order to improve the reliability of calibration signals, L. Su *at el.* used cell-edge UEs to support the calibration [28], and C. Chen *at el.* exploited maximum ratio combining and maximum ratio transmitting methods to combine calibration signals [29]. For reducing the overhead of the CSI feedback among BSs, a decentralized calibration was presented based on decoupling the whole calibration problem into several BS-level subproblems in [30].

When it comes to relaying systems, the reciprocity mismatch is not only caused by the RF gains of sources and destinations, but also caused by the RF gains of relays. As a result, it results in the complicated reciprocity mismatch by exploiting relays to assist the communication in wireless multi-node networks. Hence, relays have to be involved in the reciprocity calibration. Moreover, due to the involvement of relays, the two-side reciprocity calibration becomes the three-side reciprocity calibration. This leads to a large increase of the overhead and the computational complexity of the reciprocity calibration. Consequently, both the impact analysis and calibration of the reciprocity mismatch are more challenging than those in conventional systems.

Motivated by above observations, we investigate the reciprocity mismatch in TDD relaying systems. We first derive the closed-form expression of the achievable rate with the reciprocity mismatch of all devices. Then, the impact of the mismatch at the source side, the relay side and the destination side on the system performance is analyzed respectively. The analytical results show that the mismatch at the relay side dominates the performance loss. Under the guidance of these results, we propose a two-stage reciprocity calibration consisting of intra-calibration and inter-calibration. The intra-calibration is based on hardware circuits and the inter-calibration is based on space signals with a discrete Fourier transform (DFT) codebook. After the reciprocity calibration, the achievable rate is derived to analyze the impact of the estimation errors of calibration coefficients on the system performance. We also derive the calibration gain by comparing the achievable rate before and after calibration, which demonstrates that the system performance can be improved by the proposed reciprocity calibration. The main contributions of the work are summarized as follows.

- *Impact analysis of the reciprocity mismatch:* We derive the closed-form expression of the achievable rate with the reciprocity mismatch caused by the RF gains of sources, relays, and destinations. Analytical results reveal that the reciprocity mismatch at the relay side dominates the impact.
- *Two-stage reciprocity calibration method:* To calibrate the relays, a two-stage calibration is proposed. The relays first perform the intra-calibration based on the hardware independently, followed by the inter-calibration based on a DFT codebook with the assistance of a reference relay.
- *Performance analysis after the calibration:* We derive the achievable rate after the two-stage calibration to investigate the impact of the estimation errors of calibration coefficients. Further, the calibration gain is derived to demonstrate the performance improvement of operating the proposed calibration.

The rest of the paper is organized as follows. Section II describes the system model. The impact of the reciprocity mismatch analysis is presented in Section III. In section IV, the two-stage calibration is proposed, and then, the performance after the calibration is derived. Simulations and numerical results are given in Section V, and conclusion is given in VI.

Throughout the paper, vectors and matrices are denoted in bold lowercase and uppercase respectively: $\mathbf{a}$ and $\mathbf{A}$. Let $\mathbf{A}^T$, $\mathbf{A}^H$ and $\mathbf{A}^{-1}$ denote the transpose, conjugate transpose and inverse of a matrix $\mathbf{A}$ respectively. $\mathrm{tr}(\cdot)$ stands for the trace operator and $\mathbb{E}(\cdot)$ represents the expectation operation. Let $\|\mathbf{a}\|^2$ denote the norm of the vector $\mathbf{a}$. $\otimes$ denotes the Kronecker product. $\mathrm{diag}(a_1, \cdots, a_N)$ denotes a N by N diagonal matrix with diagonal entries given by $a_1, \cdots, a_N$. $[\mathbf{A}]_{.i}$ and $[\mathbf{A}]_{k.}$ are the i-th column and k-th row of a matrix $\mathbf{A}$. $\mathcal{N}(\mu, \sigma^2)$ represents for normal distribution with mean μ and variance σ^2. $\mathcal{U}(a, b)$ denotes uniform distribution on the interval $[a, b]$.

II. System Model

In this paper, we consider a TDD relaying system illustrated in Fig. 1, which consists of K independent S-D pairs and M half-duplex amplify-and-forward relays. Both sources and destinations are equipped with the single antenna, and each relay is equipped with N antennas.

The overall channel consists of the reciprocal wireless propagation channel as well as the non-reciprocal RF gain.

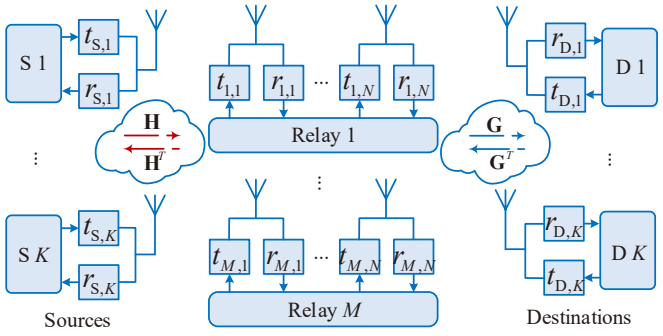

Fig. 1. A relaying system consisting of K source-destination pairs and M relays.

The reciprocal wireless propagation channel matrix between sources and relays is defined as $\mathbf{H} \in \mathbb{C}^{MN\times K}$ with the k-th column $\mathbf{h}_k = \mathbf{\Phi}_{\mathrm{h},k}^{\frac{1}{2}}\mathbf{v}_{\mathrm{h},k}$, where $\mathbf{v}_{\mathrm{h},k}$ is the Rayleigh fading channel distributed as $\mathcal{CN}(0,\mathbf{I}_{MN})$, and $\mathbf{\Phi}_{\mathrm{h},k} = \mathrm{diag}(\phi_{\mathrm{h},1,k},\cdots,\phi_{\mathrm{h},M,k})\otimes\mathbf{I}_N$ with $\phi_{\mathrm{h},m,k}$ denoting the large-scale path loss between the m-th relay and the k-th source. Let $\mathbf{G} = [\mathbf{g}_1^T,\cdots,\mathbf{g}_K^T]^T \in \mathbb{C}^{K\times MN}$ be the wireless channel matrix between relays and destinations, where $\mathbf{g}_k$ is equal to $\mathbf{v}_{\mathrm{g},k}\mathbf{\Phi}_{\mathrm{g},k}^{\frac{1}{2}}$, $\mathbf{v}_{\mathrm{g},k}$ denotes the Rayleigh fading channel and obeys $\mathcal{CN}(0,\mathbf{I}_{MN})$, and $\mathbf{\Phi}_{\mathrm{g},k} = \mathrm{diag}(\phi_{\mathrm{g},1,k},\cdots,\phi_{\mathrm{g},M,k})\otimes\mathbf{I}_N$ denotes the large-scale path loss between the relays and the k-th destination. Then, the overall uplink and downlink channel can be modeled as

$$\begin{aligned}\mathbf{H}_{\mathrm{DL}} &= \mathbf{R}\mathbf{H}\mathbf{T}_{\mathrm{S}}, \quad & \mathbf{H}_{\mathrm{UL}} &= \mathbf{R}_{\mathrm{S}}\mathbf{H}^T\mathbf{T},\\ \mathbf{G}_{\mathrm{DL}} &= \mathbf{R}_{\mathrm{D}}\mathbf{G}\mathbf{T}, \quad & \mathbf{G}_{\mathrm{UL}} &= \mathbf{R}\mathbf{G}^T\mathbf{T}_{\mathrm{D}},\end{aligned} \tag{1}$$

where $\mathbf{T}_{\mathrm{s}} = \mathrm{diag}(t_{\mathrm{s},1},\cdots,t_{\mathrm{s},K})$, $\mathbf{R}_{\mathrm{s}} = \mathrm{diag}(r_{\mathrm{s},1},\cdots,r_{\mathrm{s},K})$, $t_{\mathrm{S},k}$ and $r_{\mathrm{S},k}$ respectively denote the transmit and receive RF gains of the k-th source, $\mathbf{T}_{\mathrm{D}} = \mathrm{diag}(t_{\mathrm{D},1},\cdots,t_{\mathrm{D},K})$, $\mathbf{R}_{\mathrm{D}} = \mathrm{diag}(r_{\mathrm{D},1},\cdots,r_{\mathrm{D},K})$, $t_{\mathrm{D},k}$ and $r_{\mathrm{D},k}$ are the transmit and receive RF gains of the k-th destination, $\mathbf{T} = \mathrm{diag}(t_{1,1},\cdots,t_{M,N})$ and $\mathbf{R} = \mathrm{diag}(r_{1,1},\cdots,r_{M,N})$, $t_{m,n}$ and $r_{m,n}$ denote the transmit and receive RF gains of the n-th antenna in the m-th relay. The amplitudes of RF gains can be modeled as log-normal distribution and their phases can be modeled as uniform distribution [24]. Hence, the RF gains can be characterized as

$$\begin{aligned}t_{\mathrm{S},k} &= |t_{\mathrm{S},k}|e^{j\varphi_{\mathrm{S},k}^{(\mathrm{t})}}, r_{\mathrm{S},k} = |r_{\mathrm{S},k}|e^{j\varphi_{\mathrm{S},k}^{(\mathrm{r})}},\\ t_{m,n} &= |t_{m,n}|e^{j\varphi_{m,n}^{(\mathrm{t})}}, r_{m,n} = |r_{m,n}|e^{j\varphi_{m,n}^{(\mathrm{r})}},\\ t_{\mathrm{D},k} &= |t_{\mathrm{D},k}|e^{j\varphi_{\mathrm{D},k}^{(\mathrm{t})}}, r_{\mathrm{D},k} = |r_{\mathrm{D},k}|e^{j\varphi_{\mathrm{D},k}^{(\mathrm{r})}},\end{aligned} \tag{2}$$

with

$$\begin{aligned}&\ln|t_{\mathrm{S},k}| \sim \mathcal{N}(0,\delta_{\mathrm{S,t}}^2), \varphi_{\mathrm{S},k}^{(\mathrm{t})} \sim \mathcal{U}(-\theta_{\mathrm{S,t}},\theta_{\mathrm{S,t}}),\\ &\ln|r_{\mathrm{S},k}| \sim \mathcal{N}(0,\delta_{\mathrm{S,r}}^2), \varphi_{\mathrm{S},k}^{(\mathrm{r})} \sim \mathcal{U}(-\theta_{\mathrm{S,r}},\theta_{\mathrm{S,r}}),\\ &\ln|t_{m,n}| \sim \mathcal{N}(0,\delta_{\mathrm{t}}^2), \varphi_{m,n}^{(\mathrm{t})} \sim \mathcal{U}(-\theta_{\mathrm{t}},\theta_{\mathrm{t}}),\\ &\ln|r_{m,n}| \sim \mathcal{N}(0,\delta_{\mathrm{r}}^2), \varphi_{m,n}^{(\mathrm{r})} \sim \mathcal{U}(-\theta_{\mathrm{r}},\theta_{\mathrm{r}}),\\ &\ln|t_{\mathrm{D},k}| \sim \mathcal{N}(0,\delta_{\mathrm{D,t}}^2), \varphi_{\mathrm{D},k}^{(\mathrm{t})} \sim \mathcal{U}(-\theta_{\mathrm{D,t}},\theta_{\mathrm{D,t}}),\\ &\ln|r_{\mathrm{D},k}| \sim \mathcal{N}(0,\delta_{\mathrm{D,r}}^2), \varphi_{\mathrm{D},k}^{(\mathrm{r})} \sim \mathcal{U}(-\theta_{\mathrm{D,r}},\theta_{\mathrm{D,r}}).\end{aligned} \tag{3}$$

The communication process of S-D pairs is conducted in two phases minutely described as follows.

In the first communication phase, sources transmit signals to relays. Let $\mathbf{x}_{\mathrm{S}} = [x_{\mathrm{S},1},\cdots,x_{\mathrm{S},K}]^T \in \mathbb{C}^K$ be the signals transmitted by sources with $\mathbb{E}\{|x_{\mathrm{S},k}|^2\} = 1$. The received signal vector at all relays is denoted as

$$\mathbf{x}_{\mathrm{R}} = \sqrt{\rho_1}\mathbf{H}_{\mathrm{DL}}\mathbf{x}_{\mathrm{S}} + \mathbf{n}_{\mathrm{R}}, \tag{4}$$

where $\mathbf{x}_{\mathrm{R}} \in \mathbb{C}^{MN}$ is the received signal vector, ρ_1 is the common transmit power of the first communication phase and $\mathbf{n}_{\mathrm{R}} \in \mathbb{C}^{MN}$ is the additive white Gaussian noise (AWGN) vector at relays with each entry distributed as $\mathcal{CN}(0,\sigma_{\mathrm{rn}}^2)$.

In the second communication phase, relays transmit the received signal $\mathbf{x}_{\mathrm{R}}$ to destinations by amplifying and cooperative beamforming. And the received signal vector $\mathbf{y} = [y_1,\cdots,y_K]^T \in \mathbb{C}^K$ at destinations can be given by

$$\mathbf{y} = \mathbf{G}_{\mathrm{DL}}\mathbf{W}\mathbf{x}_{\mathrm{R}} + \mathbf{n}_{\mathrm{y}}, \tag{5}$$

where $\mathbf{n}_{\mathrm{y}} = [n_{\mathrm{y},1},\cdots,n_{\mathrm{y},K}]^T \in \mathbb{C}^K$ is the received AWGN vector with the entries distributed as $\mathcal{CN}(\mathbf{0},\sigma_{\mathrm{yn}}^2\mathbf{I}_K)$ and $\mathbf{W}$ denotes the beamforming matrix. To reduce the interference among the S-D pairs, the beamforming matrix based on ZF criterion is given by [31]

$$\mathbf{W} = \sqrt{\rho_2\beta}\underbrace{\mathbf{G}_{\mathrm{UL}}^*(\mathbf{G}_{\mathrm{UL}}^T\mathbf{G}_{\mathrm{UL}}^*)^{-1}}_{\mathbf{W}_{\mathrm{G}}}\underbrace{(\mathbf{H}_{\mathrm{DL}}^H\mathbf{H}_{\mathrm{DL}})^{-1}\mathbf{H}_{\mathrm{DL}}^H}_{\mathbf{W}_{\mathrm{H}}}, \tag{6}$$

where ρ_2 is the common transmit power of the second communication phase, $\mathbf{W}_{\mathrm{H}}$ transforms the signal received at relays into parallel streams, $\mathbf{W}_{\mathrm{G}}$ denotes the precoding matrix of the second communication phase and β is the normalization scalar of the transmit signals at relays defined as [31]

$$\beta = 1/\mathbb{E}\left\{\|\mathbf{W}_{\mathrm{G}}\mathbf{W}_{\mathrm{H}}\mathbf{x}_{\mathrm{R}}\|^2\right\}. \tag{7}$$

III. Impact of Reciprocity Mismatch

In this section, the closed-form expression of the ergodic achievable rate is first derived with the reciprocity mismatch. Then, we further analyze the impact of the mismatch on the system performance. Finally, the impacts of the reciprocity mismatch caused by the RF gains of sources, relays and destinations are discussed and compared.

A. Achievable Rate with Reciprocity Mismatch

According to (4) and (5), the received signal at the k-th $(k = 1,\cdots,K)$ destination can be further written as

$$y_k = \underbrace{\sqrt{\rho_1}b_{k,k}x_{\mathrm{S},k}}_{\mathrm{ES}_k} + \underbrace{\sqrt{\rho_1}\sum_{i=1,i\neq k}^{K} b_{k,i}x_{\mathrm{S},i}}_{\mathrm{IDI}_k} + \underbrace{\tilde{n}_{\mathrm{r},k} + n_{\mathrm{y},k}}_{\mathrm{RN}_k}, \tag{8}$$

with $\mathbf{b}_k = [b_{k,1},\cdots,b_{k,K}] = \sqrt{\rho_2\beta}\mathbf{g}_{\mathrm{DL},k}\mathbf{W}_{\mathrm{G}}$ and $\tilde{n}_{\mathrm{r},k} = \mathbf{g}_{\mathrm{DL},k}\mathbf{W}\mathbf{n}_{\mathrm{R}}$, where $b_{k,k}$ is the k-th entry of $\mathbf{b}_k$ and denotes the equivalent channel gain of the k-th destination, $b_{k,i}$ is the i-th $(i \neq k)$ entry of $\mathbf{b}_k$ and denotes the correlation between the k-th destination and the i-th destination, ES_k is the effective signal, IDI_k represents the inter-destination-interference (IDI),

RN_k denotes the equivalent received noise at k-th destination due to both the first and second communication phases.

The achievable rate of the k-th S-D pair can be defined as

$$R_k = \mathbb{E}\left\{\log\left(1+\gamma_k\right)\right\}, \tag{9}$$

where

$$\gamma_k = \frac{\rho_1 |b_{k,k}|^2}{\rho_1 \sum_{i\neq k}^{K} |b_{k,i}|^2 + \sigma_{\mathrm{rn}}^2 \|\mathbf{g}_{\mathrm{DL},k}\mathbf{W}\|^2 + \sigma_{\mathrm{yn}}^2} \tag{10}$$

denotes the signal-to-interference-plus-noise ratio (SINR). Then, the closed-form expression of the achievable rate can be given as Proposition 1.

Proposition 1 (Achievable rate with reciprocity mismatch)**.** With assumption that both MN and K are large, a lower bound of the achievable rate of the k-th $(k = 1, \cdots, K)$ S-D pair can be given by

$$R_{\mathrm{L},k} = \log\left(1 + \frac{\bar{\Gamma}_k^{\mathrm{ES}}}{\bar{\Gamma}_k^{\mathrm{IDI}} + \bar{\Gamma}_k^{\mathrm{rn}} + \bar{\Gamma}_k^{\mathrm{yn}}}\right) \tag{11}$$

with

$$\begin{aligned}
\bar{\Gamma}_k^{\mathrm{ES}} &= \frac{(MN-K)(\mathrm{sinc}(\theta_{\mathrm{t}})\mathrm{sinc}(\theta_{\mathrm{r}}))^2}{e^{\delta_{\mathrm{r}}^2-\delta_{\mathrm{t}}^2}}, \\
\bar{\Gamma}_k^{\mathrm{IDI}} &= \sum_{i\neq k}^{K} \frac{e^{2\delta_{\mathrm{t}}^2} + e^{2\delta_{\mathrm{r}}^2} - 2e^{(\delta_{\mathrm{t}}^2+\delta_{\mathrm{r}}^2)/2}\mathrm{sinc}(\theta_{\mathrm{t}})\mathrm{sinc}(\theta_{\mathrm{r}})}{(MN-K)^{-1}MN\psi_{2,i}^2\psi_{3,k,i}^{-1}}, \\
\bar{\Gamma}_k^{\mathrm{rn}} &= \frac{(\mathrm{sinc}(\theta_{\mathrm{t}})\mathrm{sinc}(\theta_{\mathrm{r}}))^2\sigma_{\mathrm{rn}}^2}{\rho_1\psi_{4,k}e^{3\delta_{\mathrm{r}}^2-\delta_{\mathrm{t}}^2-2\delta_{\mathrm{S},t}^2}}
\end{aligned} \tag{12}$$

and

$$\bar{\Gamma}_k^{\mathrm{yn}} = \frac{\sigma_{\mathrm{yn}}^2\psi_1 e^{2\delta_{\mathrm{D,t}}^2}}{\rho_2}, \tag{13}$$

where $\bar{\Gamma}_k^{\mathrm{ES}}$ is the power of the effective signal, $\bar{\Gamma}_k^{\mathrm{IDI}}$ denotes the power of the IDI, $\bar{\Gamma}_k^{\mathrm{rn}}$ is the power of the equivalent received noise of the first communication phase, $\bar{\Gamma}_k^{\mathrm{yn}}$ denotes the power of the equivalent received noise of the second communication phase, $\psi_1 = \sum_{k=1}^{K}(\mathrm{tr}\{\mathbf{\Phi}_{\mathrm{g},k}\})^{-1}MN$, $\psi_{2,k} = (MN)^{-1}\mathrm{tr}\{\mathbf{\Phi}_{\mathrm{g},k}\}$, $\psi_{3,k,i} = (MN)^{-1}\mathrm{tr}\{\mathbf{\Phi}_{\mathrm{g},k}\mathbf{\Phi}_{\mathrm{g},i}\}$ and $\psi_{4,k} = (MN)^{-1}\mathrm{tr}\{\mathbf{\Phi}_{\mathrm{h},k}\}$.

Proof: See Appendix A. ∎

Based on Proposition 1, by considering a case with ideal RF chains, i.e. $\delta_{\mathrm{t}}^2 = \delta_{\mathrm{r}}^2 = \delta_{\mathrm{S,r}}^2 = \delta_{\mathrm{S,t}}^2 = \delta_{\mathrm{D,r}}^2 = \delta_{\mathrm{D,t}}^2 = 0$ and $\theta_{\mathrm{r}} = \theta_{\mathrm{t}} = \theta_{\mathrm{S,r}} = \theta_{\mathrm{S,t}} = \theta_{\mathrm{D,r}} = \theta_{\mathrm{D,t}} = 0$, the achievable rate without the reciprocity mismatch is given by

$$R_k^{\mathrm{ideal}} = \log\left(1 + \frac{\rho_1\rho_2(MN-K)}{\rho_2\sigma_{\mathrm{rn}}^2\psi_{4,k}^{-1} + \rho_1\sigma_{\mathrm{yn}}^2\psi_1}\right), \tag{14}$$

which is a benchmark of ergodic achievable rate of the relaying system with ZF beamforming.

Although the achievable rates are derived in (11) and (14), it is difficult to get significant insights from these expressions directly. Hence, further impact analysis of the reciprocity mismatch on the relaying system performance is discussed in the next section.

B. Impact Analysis of the Mismatch

By comparing $R_{\mathrm{L},k}$ with R_k^{ideal}, the performance loss can be denoted as

$$\Delta R_k = R_k^{\mathrm{ideal}} - R_{\mathrm{L},k} \overset{(a)}{\approx} \log\left(\gamma_k^{\mathrm{IDI}} + \gamma_k^{\mathrm{rn}} + \gamma_k^{\mathrm{yn}}\right), \tag{15}$$

with

$$\begin{aligned}
\gamma_k^{\mathrm{IDI}} &= \frac{(e^{2\delta_{\mathrm{t}}^2} + e^{2\delta_{\mathrm{r}}^2} - 2e^{(\delta_{\mathrm{t}}^2+\delta_{\mathrm{t}}^2)/2}\mathrm{sinc}(\theta_{\mathrm{t}})\mathrm{sinc}(\theta_{\mathrm{r}}))e^{\delta_{\mathrm{r}}^2-\delta_{\mathrm{t}}^2}}{\psi_5^{-1}(\mathrm{sinc}(\theta_{\mathrm{t}})\mathrm{sinc}(\theta_{\mathrm{r}}))^2(\sigma_{\mathrm{rn}}^2\psi_{4,k}^{-1}\rho_1^{-1} + \sigma_{\mathrm{yn}}^2\psi_1\rho_2^{-2})}, \\
\gamma_k^{\mathrm{rn}} &= \frac{\sigma_{\mathrm{rn}}^2\psi_{4,k}^{-1}\rho_1^{-1}e^{2\delta_{\mathrm{S,t}}^2-2\delta_{\mathrm{t}}^2}}{(\sigma_{\mathrm{rn}}^2\psi_{4,k}^{-1}\rho_1^{-1} + \sigma_{\mathrm{yn}}^2\psi_1\rho_2^{-2})}, \\
\gamma_k^{\mathrm{yn}} &= \frac{\sigma_{\mathrm{yn}}^2\psi_1\rho_2^{-1}e^{2\delta_{\mathrm{D,t}}^2+\delta_{\mathrm{r}}^2-\delta_{\mathrm{t}}^2}}{(\mathrm{sinc}(\theta_{\mathrm{t}})\mathrm{sinc}(\theta_{\mathrm{r}}))^2(\sigma_{\mathrm{rn}}^2\psi_{4,k}^{-1}\rho_1^{-1} + \sigma_{\mathrm{yn}}^2\psi_1\rho_2^{-2})},
\end{aligned} \tag{16}$$

where (a) holds at the high SNR regime, i.e. $\rho_1 \gg \sigma_{\mathrm{rn}}^2$ and $\rho_2 \gg \sigma_{\mathrm{yn}}^2$, and $\psi_5 = \sum_{i\neq k}^{K}\psi_{3,k,i}\psi_{2,i}^{-2}(MN-K)(MN)^{-1}$. From (16), we find that the impacts of mismatches of sources and destinations are correlated with the impact of the mismatch in relays respectively. To obtain the several impacts of reciprocity mismatches of sources, relays and destinations, we consider three special cases as follows.

Impact of reciprocity mismatch of sources: By letting RF chains of relays and destinations be ideal, i.e. $\delta_{\mathrm{r}} = \delta_{\mathrm{t}} = \delta_{\mathrm{D,r}} = \delta_{\mathrm{D,t}} = 0$ and $\theta_{\mathrm{r}} = \theta_{\mathrm{t}} = \theta_{\mathrm{D,r}} = \theta_{\mathrm{D,t}} = 0$, the performance loss ΔR_k can be rewritten as

$$\Delta R_k \approx \log\left(\frac{\rho_2 e^{2\delta_{\mathrm{S,t}}^2}\sigma_{\mathrm{rn}}^2\psi_{4,k}^{-1} + \rho_1\sigma_{\mathrm{yn}}^2\psi_1}{\rho_2\sigma_{\mathrm{rn}}^2\psi_{4,k}^{-1} + \rho_1\sigma_{\mathrm{yn}}^2\psi_1}\right), \tag{17}$$

which denotes the degradation of achievable rate only caused by the RF gains of sources. In general, sources are closer to relays than destinations [32], which indicates $(MN)^{-1}\mathrm{tr}\{\mathbf{\Phi}_{\mathrm{g},k}\} > (MN)^{-1}\mathrm{tr}\{\mathbf{\Phi}_{\mathrm{h},k}\}$. Hence, when K is large, $\psi_{4,k}^{-1} \ll \psi_1$, and then, $(\rho_2 e^{2\delta_{\mathrm{S,t}}^2}\sigma_{\mathrm{rn}}^2\psi_{4,k}^{-1} + \rho_1\sigma_{\mathrm{yn}}^2\psi_1)/(\rho_2\sigma_{\mathrm{rn}}^2\psi_{4,k}^{-1} + \rho_1\sigma_{\mathrm{yn}}^2\psi_1) \approx 1$, which implies the performance loss ΔR_k is quite small. Moreover, the amplitudes of the RF gains of sources slightly degrade the system performance by increasing the power of the equivalent received noise of the first communication phase, but the phases of the RF gains of sources do not affect the achievable rate.

Impact of reciprocity mismatch of relays: By letting RF chains of sources and destinations be ideal, i.e. $\delta_{\mathrm{S,r}} = \delta_{\mathrm{S,t}} = \delta_{\mathrm{D,r}} = \delta_{\mathrm{D,t}} = 0$ and $\theta_{\mathrm{S,r}} = \theta_{\mathrm{S,t}} = \theta_{\mathrm{D,r}} = \theta_{\mathrm{D,t}} = 0$, the performance loss ΔR_k can be rewritten as (18) at the bottom of this page, which denotes the performance loss only resulting from the reciprocity mismatch of relays, where $\psi_6 = [\rho_2 e^{\delta_{\mathrm{t}}^2-3\delta_{\mathrm{r}}^2}(\mathrm{sinc}(\theta_{\mathrm{t}})\mathrm{sinc}(\theta_{\mathrm{r}}))^2\sigma_{\mathrm{rn}}^2\psi_{4,k}^{-1} +$

$$\Delta R_k \approx \log\left(\psi_6 + \frac{e^{2\delta_{\mathrm{r}}^2} + e^{2\delta_{\mathrm{t}}^2} - 2e^{(\delta_{\mathrm{t}}^2+\delta_{\mathrm{r}}^2)/2}\mathrm{sinc}(\theta_{\mathrm{t}})\mathrm{sinc}(\theta_{\mathrm{r}})}{(\sigma_{\mathrm{rn}}^2(\psi_{4,k}\rho_1)^{-1} + \sigma_{\mathrm{yn}}^2\psi_1\rho_2^{-1})\psi_5^{-1}}\right) + \log\left(\frac{e^{\delta_{\mathrm{r}}^2-\delta_{\mathrm{t}}^2}}{(\mathrm{sinc}(\theta_{\mathrm{t}})\mathrm{sinc}(\theta_{\mathrm{r}}))^2}\right), \tag{18}$$

$\rho_1\sigma_{\rm yn}^2\psi_1]/(\rho_2\sigma_{\rm rn}^2\psi_{4,k}^{-1}+\rho_1\sigma_{\rm yn}^2\psi_1)$. According to (18), both the amplitude mismatch and the phase mismatch of relays result in IDI, which increases with transmit powers ρ_1 and ρ_2 increasing. This indicates that the reciprocity mismatch of relays causes the severe performance loss, especially at the high SNR regime.

Impact of reciprocity mismatch of destinations: By assuming that RF chain of sources and relays are ideal, i.e. $\delta_{\rm r}=\delta_{\rm t}=\delta_{\rm S,r}=\delta_{\rm S,t}=0$ and $\theta_{\rm r}=\theta_{\rm t}=\theta_{\rm S,r}=\theta_{\rm S,t}=0$, the performance loss ΔR_k can be rewritten as

$$\Delta R_k \approx \log\left(\frac{\rho_2\sigma_{\rm rn}^2\psi_{4,k}^{-1}+\rho_1 e^{2\delta_{\rm D,t}^2}\sigma_{\rm yn}^2\psi_1}{\rho_2\sigma_{\rm rn}^2\psi_{4,k}^{-1}+\rho_1\sigma_{\rm yn}^2\psi_1}\right), \qquad (19)$$

which denotes the performance loss of achievable rate only resulting from the mismatch at of destinations. When K is large and $\psi_{4,k}^{-1}\ll\psi_1$, the performance loss term ΔR_k can be further approximated as $\Delta R_k\approx\log(e^{2\delta_{\rm D,t}^2})=2(\ln 2)^{-1}\delta_{\rm D,t}^2$. Accordingly, the amplitude mismatch of destinations degrades the system performance by increasing the powers of the equivalent received noises of the second communication phase, but the phases of RF gains do not affect the achievable rate. Furthermore, as the variance $\delta_{\rm D,t}^2$ of the amplitude mismatch is limited, the performance loss is limited as well.

Remark 1 (Mismatch at relays dominate impacts)**.** In light of the above analytical results, we find that the performance loss ΔR_k resulting from the mismatch of relays increases as the transmit power increase, while the performance losses ΔR_k caused by the mismatch of both sources and destinations tend to be a constant. This implies that the performance loss caused by the mismatch at the relay side is much larger than the performance losses caused by the mismatch at the source side and the destination side at the high transmit SNR regime. Hence, the mismatch at the relay side dominates the impacts on the system performance.

To further compare performance losses of the three cases intuitively, an numerical example is given as follows. We set $MN=256$, $K=20$, and suppose that amplitudes of RF gains are distributed as $\{\ln|t|,\ln|r|\}\sim\mathcal{N}(0,0.05)$, phases are distributed as $\{\angle r,\angle t\}\sim\mathcal{U}(-0.1\pi,0.1\pi)$, $\mathbf{\Phi}_{{\rm h},k}=\mathbf{\Phi}_{{\rm g},k}=\mathbf{I}_{MN}$, $\sigma_{\rm rn}=\sigma_{\rm yn}=1$, $\rho_1=\rho_2=\rho$. From (17), the performance loss caused by the reciprocity mismatch at the source side is about $\Delta R_k=0.046$ bits/s/Hz. Based on (19), the performance loss resulting from the reciprocity mismatch at the destination side is $\Delta R_k=0.144$ bits/s/Hz. And according to (18), the performance loss caused by the reciprocity mismatch of relays is $\Delta R_k=3.85$ bits/s/Hz when $\rho=20$ dB, and $\Delta R_k=7.17$ bits/s/Hz with $\rho=30$ dB. Hence, the performance loss resulting from the reciprocity mismatch at the relay side is much larger than the performance loss caused by the mismatch of sources and destinations, especially at the high SNR regime.

IV. Calibration for Relaying System

In this section, we first model the calibration coefficients of the relaying system. To estimate the coefficients, a reciprocity calibration approach is proposed. After the calibration, the system performance is investigated.

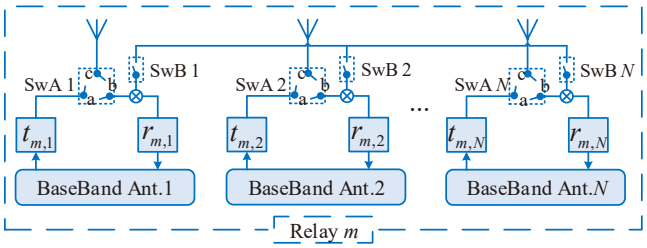

(a) Hardware circuits of intra-calibration

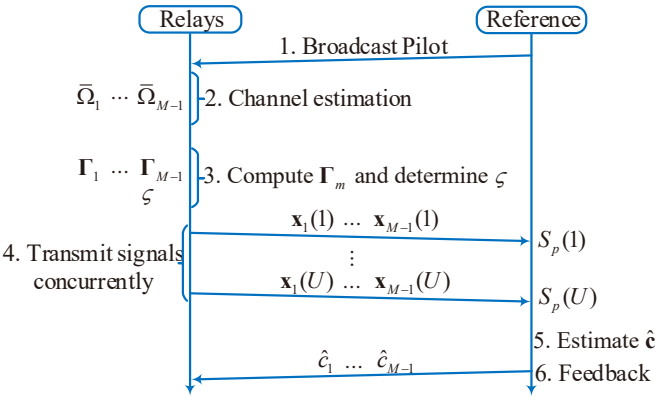

(b) Process of inter-calibration

Fig. 2. The two-stage calibration consists of the intra-calibration and inter-calibration. The intra-calibration is based on the hardwares, and the inter-calibration is based on the signal-space calibration.

According to the analyses and comparisons in Section III-B, the reciprocity mismatch at the relay side dominates the impact on the system performance. Consequently, to compensate the system performance loss and reduce the overhead of calibration, we propose a two-stage calibration approach for relays. The two stages are intra-calibration and inter-calibration respectively. The calibration coefficients also consist of the intra-calibration coefficients and inter-calibration coefficients. The calibration coefficients matrix $\mathbf{F}_m(m=1,\cdots,M)$ of m-th relay is given by

$$\mathbf{F}_m = c_m\mathbf{F}_m^{\rm iac} = c_m{\rm diag}(f_{m,1}^{\rm iac},\cdots,f_{m,N}^{\rm iac}), \qquad (20)$$

where $f_{m,n}^{\rm iac}$ denotes the intra-calibration coefficient of the n-th antennas in the m-th relay and c_m is the inter-calibration coefficients of the m-th relay. When the first antenna in the m-th relay is regarded as the reference of the intra-calibration, $f_{m,n}^{\rm iac}=\alpha_m\frac{t_{m,n}}{r_{m,n}}$ where $\alpha_m=\frac{r_{m,1}}{t_{m,1}}$. If the reference relay of the inter-calibration is the $M_{\rm ref}$-th relay, $c_m=\frac{\alpha_{M_{\rm ref}}}{\alpha_m}$.

A. Intra-calibration Based on Hardware

To obtain the intra-calibration coefficients and to reduce the signaling overhead of calibration, we present an intra-calibration following the idea of the hardware-circuit calibration in [15], [16]. The hardware-circuit calibration requires extra circuits to connect uncalibrated antennas, which is illustrated in Fig. 2a. The intra-calibration is done in 3 steps described as Algorithm 1.

Algorithm 1 Intra-calibration of the relays

- **Step 1 (Antenna self connection):** SwA $n(n = 1, \cdots, N)$ connects spot a and spot b, and SwB $n(n = 1, \cdots, N)$ disconnects. The baseband of each antenna, e.g., the n-th antenna, transmits a known signal p^{iac} simultaneously. Assuming the gain of wires is 1, the received signal is denoted as $y_{m,n}^{\text{sc}} = r_{m,n}t_{m,n}p^{\text{iac}} + z_{m,n}^{\text{sc}}$, where $z_{m,n}^{\text{sc}}$ denotes the thermal noise.
- **Step 2 (Antenna parallel connection):** SwA 1 holds the connection, while SwA $n(n = 2, \cdots, N)$ disconnects, and SwB $n(n = 1, \cdots, N)$ connects. The baseband of the first antenna transmit the signal p^{iac} to other antennas, the received signal at the baseband of the n-th antenna is given as $y_{m,n}^{\text{pc}} = t_{m,1}r_{m,n}p^{\text{iac}} + z_{m,n}^{\text{pc}}$, where $z_{m,n}^{\text{pc}}$ is the thermal noise.
- **Step 3 (Coefficients calculation):** The intra-calibration coefficients is computed as $\hat{f}_{m,n}^{\text{iac}} = y_{m,n}^{\text{sc}} y_{m,1}^{\text{sc}} / (y_{m,n}^{\text{pc}})^2$. Since the SNR of the calibration signals is usually high, the estimating error is small, and hence, $\hat{f}_{m,n}^{\text{iac}} \approx f_{m,n}^{\text{iac}}$.

Since the signaling overhead is expressed by the number of the slots for transmitting calibration signals, the overhead of the intra-calibration is 2. Additionally, the computational complexity mainly results from plenty of multiplications. Because calculating each intra-calibration coefficient requires 3 multiplications, the asymptotic computational complexity of the intra-calibration is $\mathcal{O}(N)$.

B. Inter-calibration Based on Space Signals

To obtain the inter-calibration coefficients, the calibration requires uncalibrated relays to communicate with the reference. This indicates that only the signal-space calibration can be deployed for the inter-calibration. However, during the signal-sapace calibration, fading channels and additive noises severely degrade the SNR of calibration signals. Multi-node systems use codebooks to improve SNR [33]. Hence, we propose a signal-space calibration based on a classical codebook, i.e., DFT codebook [34]. Moreover, to avoid the overhead of CSI feedback, the local ZF beamforming can be used for the channel pre-equalization. As shown in Fig. 2b, the inter-calibration is done in 6 steps and can be described as Algorithm 2.

Algorithm 2 Inter-calibration of the relays

- **Step 1 (Pilots broadcasting from reference):** We regard the M-th relay as the reference relay, where the number of the antennas that participating in the inter-calibration is $Q(1 \leq Q \leq N)$. The antennas broadcast the pilots whose power is ρ_c to the uncalibrated relays in turn.
- **Step 2 (Channel estimation at relays):** Each uncalibrated relay, i.e, m-th relay, estimates the channel by LS method as $\hat{\mathbf{\Omega}}_{\text{DL},m} = \sqrt{\phi_{m,M}}\mathbf{R}_m\mathbf{\Omega}_m\mathbf{T}_M + \tilde{\mathbf{Z}}_{\text{DL},m}$, where $\mathbf{T}_M = \text{diag}(t_{M,1}, \cdots, t_{M,N})$, $\mathbf{\Omega}_m$ is the wireless channel, $\phi_{m,M}$ denotes the large-scale path loss between the reference and m-th relay, and $\tilde{\mathbf{Z}}_{\text{DL},m}$ is the estimation error with each entry distributed as $\mathcal{CN}(0, \sigma_z^2/\rho_c)$. Then, the estimated CSI is calibrated by the intra-calibration matrix $\hat{\mathbf{F}}_m^{\text{iac}}$, and the equivalent CSI after intra-calibration is denoted as

$$\bar{\mathbf{\Omega}}_m = \hat{\mathbf{F}}_m^{\text{iac}}\hat{\mathbf{\Omega}}_{\text{DL},m} = \mathbf{\Omega}_m^{\text{iac}} + \tilde{\mathbf{Z}}_m^{\text{iac}}, \tag{21}$$

  where $\mathbf{\Omega}_m^{\text{iac}} = \sqrt{\phi_{m,M}}\alpha_m\mathbf{T}_m\mathbf{\Omega}_m\mathbf{T}_M$ with $\mathbf{T}_m = \text{diag}(t_{m,1}, \cdots, t_{m,N})$ and $\tilde{\mathbf{Z}}_m^{\text{iac}} = \hat{\mathbf{F}}_m^{\text{iac}}\tilde{\mathbf{Z}}_{\text{DL},m}$.
- **Step 3 (Compute beamforming matrix and power scalar):** The local ZF beamforming matrix of m-th relay is denoted as $\mathbf{\Gamma}_m = \bar{\mathbf{\Omega}}_m^*(\bar{\mathbf{\Omega}}_m^T\bar{\mathbf{\Omega}}_m^*)^{-1}$. Then, the power control scalar $\varsigma = \min_m \left\{1/\text{tr}(\mathbf{\Gamma}_m^H\mathbf{\Gamma}_m)\right\}$ is determined by [35, Aglorithm 2].
- **Step 4 (Transmit calibration signals concurrently):** Let $p(m,u) = e^{-j\frac{2\pi}{M-1}(m-1)(u-1)}(u = 1, \cdots, M-1)$ denote the DFT codebook of the m-th relay during the u-th transmission. And the calibration signal vector during the u-th transmission is given as $\mathbf{x}_m(u) = \sqrt{\eta}\mathbf{\Gamma}_m\mathbf{1}_Q p(m,u)$, where $\eta = \rho_c\varsigma$, $\mathbf{1}_Q = [1, \cdots, 1]^T \in \mathbb{R}^Q$. After the relays transmit the calibration signals concurrently, the received calibration signal during the u-th$(u = 1, \cdots, M-1)$ transmission at the reference is given as

$$S_p(u) = \mathbf{b}_{\text{r}}^T \sum_{m=1}^{M-1} \mathbf{\Omega}_{\text{UL},m}\mathbf{x}_m(u) + \mathbf{b}_{\text{r}}^T\mathbf{z}_{\text{UL}}(u), \tag{22}$$

  where $\mathbf{b}_{\text{r}} = \frac{1}{Q\sqrt{\eta}}\hat{\mathbf{F}}_M^{\text{iac}}\mathbf{1}_Q$ is the receive vector, $\mathbf{\Omega}_{\text{UL},m} = \sqrt{\phi_{m,M}}\mathbf{R}_M\mathbf{\Omega}_m^T\mathbf{T}_m$ denotes the channel from the m-th relay to the reference and $\mathbf{z}_{\text{UL}}(u)$ is the complex AWGN with each entry distributed as $\mathcal{CN}(0, \sigma_z^2)$.
- **Step 5 (Inter-calibration coefficients estimation):** After the uncalibrated relays transmit $M-1$ times calibration signals to the reference, the inter-calibration coefficients can be estimated at the reference based on the received signals by Proposition 2.
- **Step 6 (Feedback the calibration coefficients):** The reference transmits the calibration coefficients to the relays.

Proposition 2 (Calibration coefficients estimation)**.** Based on the received signals at the reference, the calibration coefficients vector can be computed by

$$\hat{\mathbf{c}} = \mathbf{A}^{-1}\mathbf{s}_{\text{p}}, \tag{23}$$

where $\mathbf{s}_p = [S_p(1), \cdots, S_p(M-1)]^T$ and $\mathbf{A}^{-1}$ is a $M-1$ by $M-1$ matrix with the entry $[\mathbf{A}]_{\bar{n},\bar{k}} = e^{-j\frac{2\pi}{M-1}(\bar{n}-1)(\bar{k}-1)}(\bar{n} = 1, \cdots, M-1, \bar{k} = 1, \cdots, M-1)$.

Proof: See Appendix B. ■

From (23), we find that the matrix $\mathbf{A}$ is the $M-1$ point DFT matrix. Hence, the inter-calibration coefficients can be computed by the inverse fast Fourier transform (IFFT) of $\mathbf{s}_{\text{p}}$ as $\hat{\mathbf{c}} = (M-1)\text{IFFT}\{\mathbf{s}_{\text{p}}\}$. The computational complexity of the $M-1$ point IFFT is $\frac{1}{2}(M-1)\log(M-1)$, which is much smaller than that of computing the inverse matrix.

According to (20), the calibration coefficient $c_m(m = 1, \cdots, M-1)$ is a ratio as $c_m = \alpha_{\text{ref}}/\alpha_m$, where α_{ref} is the actual inter-calibration coefficient of the reference. Hence, when the M-th relay is set to the reference, the inter-calibration coefficient c_M is 1 since $c_M = \alpha_M/\alpha_M = 1$.

Remark 2 (Overhead of the inter-calibration)**.** The total signaling overhead consists of over-the-air signaling overhead and backhaul signaling overhead. Since the antennas of the reference broadcast pilots in turn and the uncalibrated relays transmit signals whose length is $M-1$ to the reference concurrently, the over-the-air signaling is given by $Q+M-1$. The overhead of determining the power scalar ς is a constant related to the bit width L of the quantization and is denoted as $L+2$ [35]. Because the reference relay feeds back the estimated calibration coefficients to other relays, the backhaul overhead is denoted as $M-1$. Hence, the overhead of the inter-calibration is given as $2(M-1)+Q+L+2$, which is linearly proportional to the number M of the relays.

Remark 3 (Computational complexity of the inter-calibration)**.** Each uncalibrated relay requires QN multiplications to calculate the equivalent CSI $\bar{\mathbf{\Omega}}_m$, and $(M-1)NQ+2Q^2N+\frac{1}{3}Q^3$ multiplications to calculate the transmit signal $\mathbf{x}_m(u)(u=1,\cdots,M-1)$. Then, the asymptotic computational complexity at each relay is $\mathcal{O}(MNQ+Q^2N+Q^3)$. At the reference, the times of multiplications is $\frac{1}{2}(M-1)\log[(M-1)]$ due to computing the calibration coefficients by the IFFT. Similarly, the asymptotic complexity is given as $\mathcal{O}(M\log M)$. Hence, the asymptotic computational complexity of the inter-calibration is given as $\max\left\{\mathcal{O}(MNQ+Q^2N+Q^3),\mathcal{O}(M\log M)\right\}$.

C. Performance Analysis of the Reciprocity Calibration

According to Proposition 2, the estimated inter-calibration coefficients vector is denoted as

$$\hat{\mathbf{c}}=\mathbf{c}+\mathbf{e}, \tag{24}$$

with the estimation errors of the inter-calibration coefficients denoted as $\mathbf{e}=\mathbf{A}^{-1}\tilde{\mathbf{z}}_{\mathrm{UL}}-\mathbf{\Upsilon}\mathbf{c}$, where $\tilde{\mathbf{z}}_{\mathrm{UL}}=[\mathbf{b}_{\mathrm{r}}^T\mathbf{z}_{\mathrm{UL}}(1),\cdots,\mathbf{b}_{\mathrm{r}}^T\mathbf{z}_{\mathrm{UL}}(M-1)]^T$ and $\mathbf{\Upsilon}=\mathrm{diag}(\tau_1,\cdots,\tau_{M-1})$ with $\tau_m=Q^{-1}\mathbf{1}_Q^T(\tilde{\mathbf{Z}}_m^{\mathrm{iac}})^T\mathbf{\Gamma}_m\mathbf{1}_Q$. Based on (20), the channel of m-th relay after the reciprocity calibration is denoted as

$$\hat{\mathbf{F}}_m=\hat{c}_m\hat{\mathbf{F}}_m^{\mathrm{iac}}=(c_m+e_m)\mathbf{F}_m^{\mathrm{iac}}, \tag{25}$$

where $e_m(m=1,\cdots,M-1)$ is the m-th entry of $\mathbf{e}$ and $e_M=0$. After reciprocity calibration, the equivalent channel is denoted as $\bar{\mathbf{G}}=\hat{\mathbf{F}}\mathbf{G}_{\mathrm{UL}}$, where $\hat{\mathbf{F}}=\mathrm{diag}(\hat{\mathbf{F}}_1,\cdots,\hat{\mathbf{F}}_M)$. Then, by substituting the equivalent channel into the beamforming matrix, the achievable rate after the reciprocity calibration is given as follows.

Proposition 3 (Achievable rate after calibration)**.** With assumption that N and Q are large, a lower bound of the achievable rate can be given by

$$R_{\mathrm{L},k}^{\mathrm{cal}}=\log\left(1+\frac{\bar{\Gamma}_{\mathrm{cal},k}^{\mathrm{ES}}}{\bar{\Gamma}_{\mathrm{cal},k}^{\mathrm{IDI}}+\bar{\Gamma}_{\mathrm{cal},k}^{\mathrm{rn}}+\bar{\Gamma}_{\mathrm{cal},k}^{\mathrm{yn}}}\right) \tag{26}$$

with

$$\begin{aligned}\bar{\Gamma}_{\mathrm{cal},k}^{\mathrm{ES}}&=\frac{(MN-K)e^{2\delta_{\mathrm{t}}^2}|1-\lambda_\tau|^2}{1+\lambda_{\tau^2}-\lambda_\tau+e^{2\delta_{\mathrm{t}}^2+2\delta_{\mathrm{r}}^2}\lambda_{\tilde{n}}},\\ \bar{\Gamma}_{\mathrm{cal},k}^{\mathrm{IDI}}&=\sum_{i\neq k}^{K}\frac{(MN-K)(\lambda_{\tau^2}+e^{2\delta_{\mathrm{t}}^2+2\delta_{\mathrm{r}}^2}\lambda_{\tilde{n}})}{MN(e^{2\delta_{\mathrm{t}}^2}\psi_{3,k,i})^{-1}\psi_{2,i}^2},\\ \bar{\Gamma}_{\mathrm{cal},k}^{\mathrm{rn}}&=\frac{|1-\lambda_\tau|^2e^{2\delta_{\mathrm{S},t}^2}\psi_{4,k}^{-1}\sigma_{\mathrm{rn}}^2}{\rho_1(1+\lambda_{\tau^2}-\lambda_\tau+e^{2\delta_{\mathrm{t}}^2+2\delta_{\mathrm{r}}^2}\lambda_{\tilde{n}})}\end{aligned} \tag{27}$$

and

$$\bar{\Gamma}_{\mathrm{cal},k}^{\mathrm{yn}}=\frac{e^{2\delta_{\mathrm{D},t}^2}\psi_1\sigma_{\mathrm{yn}}^2}{\rho_2}, \tag{28}$$

where $\lambda_\tau=\frac{1}{M-1}\sum_{m=1}^{M-1}1/[\rho_c\phi_{m,M}/(\sigma_z^2e^{2\delta_{\mathrm{t}}^2+2\delta_{\mathrm{r}}^2})+1]$, $\lambda_{\tau^2}=\frac{1}{M-1}\sum_{m=1}^{M-1}1/[\rho_c\phi_{m,M}/(\sigma_z^2e^{2\delta_{\mathrm{t}}^2+2\delta_{\mathrm{r}}^2})+1]^2$ and $\lambda_{\tilde{n}}=\sigma_z^2e^{2\delta_{\mathrm{r}}^2-2\delta_{\mathrm{t}}^2}\min_m\{\phi_{M,m}\}/[\rho_c(M-1)(N-Q+1)]$.

Proof: See Appendix C. ∎

Remark 4 (Calibration gain)**.** According to $R_{\mathrm{L},k}^{\mathrm{cal}}$ in (26) and the achievable rate R_k in (11), the calibration gain at the high SNR regime is approximated as

$$\begin{aligned}G_k^{\mathrm{cal}}=&R_{\mathrm{L},k}^{\mathrm{cal}}-R_{\mathrm{L},k}\\ \approx&\log\left(\frac{(\varepsilon_1+\varepsilon_2\rho_1^{-1}+\varepsilon_3\rho_2^{-1})\varepsilon_5}{\varepsilon_4\rho_c^{-1}+\varepsilon_2\rho_1^{-1}+\varepsilon_3\rho_2^{-1}}\right),\end{aligned} \tag{29}$$

where $\varepsilon_1=\bar{\Gamma}_k^{\mathrm{IDI}}$, $\varepsilon_2=e^{2\delta_{\mathrm{S},t}^2}\sigma_{\mathrm{rn}}^2\psi_{4,k}^{-1}$, $\varepsilon_3=\sigma_{\mathrm{yn}}^2\psi_1e^{2\delta_{\mathrm{D},t}^2}$, $\varepsilon_4=(MN-K)\min_m\{\phi_{M,m}\sum_{i\neq k}^{K}\psi_{3,k,i}[(M-1)(N-Q+1)\psi_{2,i}^2]^{-1}\}(MN)^{-1}e^{4\delta_{\mathrm{t}}^2+2\delta_{\mathrm{r}}^2}\sigma_z^2$ and $\varepsilon_5=e^{\delta_{\mathrm{t}}^2+\delta_{\mathrm{r}}^2}(\mathrm{sinc}(\theta_{\mathrm{t}})\mathrm{sinc}(\theta_{\mathrm{r}}))^{-2}$. From (29), the calibration gain increases when the SNRs of both the transmit signals and the calibration signals increase. Hence, if ρ_c, ρ_1 and ρ_2 are large enough, the calibration gain $G_c>0$. It also implies that, at the high SNR regime, the reciprocity calibration is more necessary to compensate the system performance loss caused by the reciprocity mismatch.

By comparing R_k^{cal} with R_k^{ideal} in (14), we find that the imperfect calibration can not compensate the performance degradation completely because of the estimation errors of the calibration coefficients. At high SNR regime, the performance loss of imperfect calibration is approximated as

$$\begin{aligned}\Delta R_k^{\mathrm{cal}}=&R_k^{\mathrm{ideal}}-R_{\mathrm{L},k}^{\mathrm{cal}}\\ \approx&\log\left(\mu_1+\frac{\rho_1\rho_2\mu_2\left(\rho_{\mathrm{c}}-\mu_3\right)^{-1}}{\sigma_{\mathrm{rn}}^2\rho_2\psi_{4,k}^{-1}+\sigma_{\mathrm{yn}}^2\psi_1\rho_1}\right),\end{aligned} \tag{30}$$

where $\mu_1=e^{2\delta_{\mathrm{D},t}^2}$, $\mu_2=\min_m\{\phi_{M,m}\}(MN-K)\sigma_z^2e^{2\delta_{\mathrm{t}}^2+2\delta_{\mathrm{r}}^2}\sum_{i\neq k}^{K}\psi_{3,k,i}[MN(M-1)(N-Q+1)\psi_{2,i}^2]^{-1}$ and $\mu_3=2\sigma_z^2e^{2\delta_{\mathrm{t}}^2+2\delta_{\mathrm{r}}^2}\frac{1}{M-1}\sum_{m=1}^{M-1}\phi_{m,M}$. According to (30), $\Delta R_k^{\mathrm{cal}}$ decreases as the calibration SNR ρ_c/σ_z^2 increases, but increases with the transmit SNR increasing, which implies that the calibration requires higher calibration SNR at the higher transmit SNR regime.

Further, the location of the reference has impact on the large-scale path loss $\phi_{m,M_{\mathrm{ref}}}$ between the uncalibrated relays and the reference relay, where M_{ref} is the index of the

reference. Further, $\phi_{m,M_{\text{ref}}}$ determines τ_m and the power scalar ς, which affect the performance after calibration. Accordingly, the reference can be determined by minimizing the performance loss ΔR_k^{cal}.

Proposition 4 (Selection of the inter-calibration reference)**.** When the positions of all relays are known globally, the reference relay can be selected by

$$M_{\text{ref}} = \arg\min_{o} \left\{ \frac{\max_m \left\{ d_{m,o}^{\xi} \right\}}{v_1 - \frac{1}{M} \sum_{m=1}^{M} d_{m,o}^{\xi}} \right\}, \ o = 1, \cdots, M, \tag{31}$$

where $v_1 = \zeta \rho_c / (2\sigma_z^2 e^{2\delta_{\text{t}}^2 + 2\delta_{\text{r}}^2})$ denoting a constant unrelated to the reference, ζ is the median of the mean path gain at 1 km, $d_{m,o}$ is the distance between the node m and the node o, and ξ is the path loss exponent.

Proof: The reference can be determined by minimizing the performance loss as $M_{\text{ref}} = \arg\min \left\{ \Delta R_k^{\text{cal}} \right\}$. Since only μ_2 and μ_3 in ΔR_k^{cal} are related to the large-scale path loss, the equivalent express can be denoted as

$$M_{\text{ref}} = \arg\min \left\{ \frac{\mu_2}{\rho_c - \mu_3} \right\}. \tag{32}$$

The path loss gain can be modeled as $\phi_{m,o} = \zeta d_{m,o}^{-\xi}$, where ζ is the median of the mean path gain at 1 km, $d_{m,o}$ is the distance between node m and node o, ξ is the path loss exponent [36]. By substituting $\phi_{m,o}$ into (32) and separating the multiplicative constants, the reference of the inter-calibration is determined by (31). ■

As relays know the positions of each other as well as the parameters of the large-scale path loss, the reference can be determined by the numerical computation of (31).

V. Simulation Results and Discussions

In this section, we use Monte Carlo simulations with the average of 10000 independent channel and mismatch realizations to investigate the impact of the reciprocity mismatch on the system performance and to verify the theoretical analysis in Section III. The proposed two-stage calibration in Section IV is also verified by simulation compared with a previous work.

The system parameters for simulations are set as follows. A relaying system consisting of $M = 16$ relays and $K = 20$ S-D pairs is considered. Each relay is equipped with $N = 20$ antennas. The cell radius is normalized to 1 and the minimum distance between any two nodes is set to 0.01 [36]. In the simulation, the path loss between the k-th source and m-th relay is modeled as $\phi_{\text{h},m,k} = \zeta d_{\text{h},m,k}^{-\xi}$, where ζ is the median of the mean path gain at 1 km, $d_{\text{h},m,k}$ is the distance between the source k and the relay m, and ξ is the path loss exponent [36]. Similarly, the path loss between the m-th relay and k-th destination can be given by $\phi_{\text{g},m,k} = \zeta d_{\text{g},m,k}^{-\xi}$, where $d_{\text{g},m,k}$ is the distance between the relay m and the destination k. We set the path loss exponent ξ to be 4 and assume parameter ζ to be 1. The amplitudes of all RF gains are distributed as $\{\ln|r|, \ln|t|\} \sim \mathcal{N}(0, \delta^2)$ and the phases of all RF gains are distributed as $\{\angle r, \angle t\} \sim \mathcal{U}(-\theta, \theta)$. In simulations, we set that $\sigma_{\text{rn}}^2 = \sigma_{\text{yn}}^2 = \sigma_{\text{z}}^2 = 1$, and $\rho_t = \rho_1 = \rho_2$ denoting the downlink transmit SNR, and ρ_c denotes the calibration SNR.

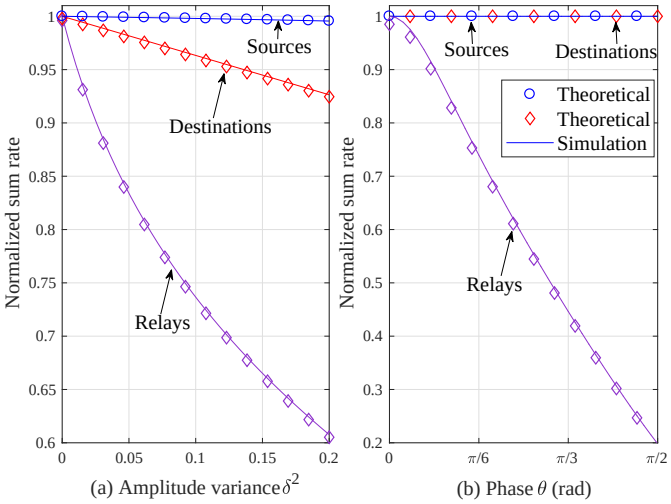

Fig. 3. Normalized sum rate with the reciprocity mismatch at relay side, destinations and sources respectively, $\rho_t = 10$ dB.

A. Impact of the Reciprocity Mismatch

To facilitate analysis, we define the normalized sum rate as $R_{\text{N}} = (\sum_{k=1}^{K} R_k)/(\sum_{k=1}^{K} R_k^{\text{ideal}})$ for every S-D pair. The impact of the amplitudes mismatch of the RF gains is illustrated in Fig. 3a for different δ^2 with the downlink transmit SNR $\rho_t = 10$ dB. From the figure, it can be seen that the achievable rates generally decrease with the increase in the variance at the relay side and the destination side, but the rate remains the constant as the amplitude variance of the RF gains at the source side increases. Compared with the ideal performance, the loss of the achievable rate is more than 25% when the amplitude variance at the relays is 0.1 and is up to 40% when the amplitude variance is 0.2. The performance loss is around 4% and 7% of the ideal case when the variance at the destinations is 0.1 and 0.2, respectively. Hence, the impact of the amplitude mismatch at relay side is much more severe than those of sources and destinations, which is consistent with the theoretical analysis in (17), (19), and (18).

The impact of the phase mismatch of the RF gain is illustrated in Fig. 3b versus the scale θ of the phase with downlink transmit SNR $\rho_t = 10$ dB. With the increase in θ of relays, the achievable rate decreases fast and almost linearly. When $\theta = \pi/6$ of the RF gains of relays, the achievable rate is about 75% of the ideal rate. And when $\theta = \pi/2$ at the relays, the rate drops to about 20% of the ideal case, which indicates that the degradation is so large. Additionally, the phases of the RF gains of sources and destinations do not affect the performance of the relaying system.

For illustrating the impact of the transmit SNR on the performance loss, we define the average performance loss as $\Delta\bar{R} = \frac{1}{K} \sum_{k=1}^{K=1} \Delta R_k$. Fig. 4 shows the average performance loss of the achievable rate versus downlink transmit SNR ρ_t in three different cases. From the illustration, it is found that the performance loss resulting from the reciprocity mismatch at the relay side increases when the downlink transmit SNR ρ_t increases, and it also increases almost linearly at the high SNR regime. The simulation result verifies the theoretical

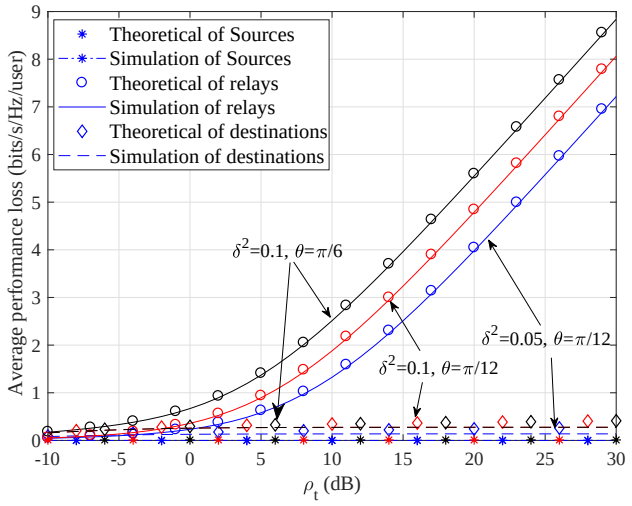

Fig. 4. Average performance loss of the achievable rate with the reciprocity mismatch versus the downlink transmit SNR ρ_t. Case 1, $\delta^2 = 0.05$, $\theta = \pi/12$; Case 2, $\delta^2 = 0.1$, $\theta = \pi/12$; Case 3, $\delta^2 = 0.1$, $\theta = \pi/6$.

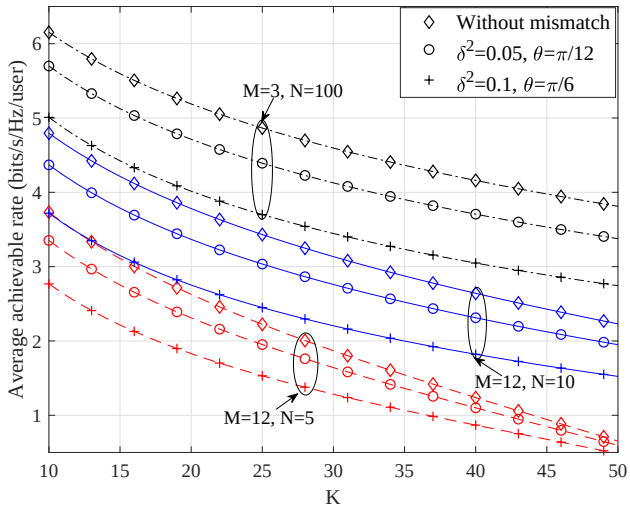

Fig. 5. Average achievable rate with the reciprocity mismatch versus the number of S-D pairs K. And the power of transmission is set to $\rho_t = 5$ dB.

analysis in (18). Additionally, the performance loss caused by the mismatch at destination side is unrelated to transmit SNR. Consequently, as analyzed in Remark 1, the performance loss caused by the reciprocity mismatch of relays is much more severe than those caused by the mismatch of both sources and destinations, especially at the high SNR regime. As a result, it is essential for reciprocity calibration at the relay side.

Finally, we illustrate how the number of S-D pairs and the number of antennas in each relay affect the average achievable rate of the relaying system. Fig. 5 shows that the achievable rate decreases with the number K of S-D pairs increasing. This is because the power allocated to each user decreasing with the increasing of K, while the multiplexing gain of the cooperative relaying system increases, which can be analytically concluded from (11). Moreover, the figure also demonstrates that the achievable rate increases slowly with the increase of antennas, which implies that the system where relays are equipped with more antennas is more robust to the reciprocity mismatch. This is because increasing the antennas of relays leads to a good condition number of the channel matrix, hence, achieves larger antenna array gain.

B. Calibration Performance

The variance of the amplitudes of RF gains is set to $\delta^2 = 0.1$ and the phases scale of the RF gains is set to $\theta = \pi/6$. The number of the antennas in the inter-calibration reference is set to $Q = N/2 = 10$. And we assume that the bit width of the power scalar ς is $L = 32$. For illustrating the effectiveness of the two-stage calibration approach proposed in this paper, we compare it with the existing work in [27]. The calibration approach is called hierarchical calibration proposed for the distributed MIMO, where BSs are distributed and similar to relays. The hierarchical calibration reduces the overhead and computational complexity of the reciprocity calibration to a certain degree, but it does not deal with fading channels and noises.

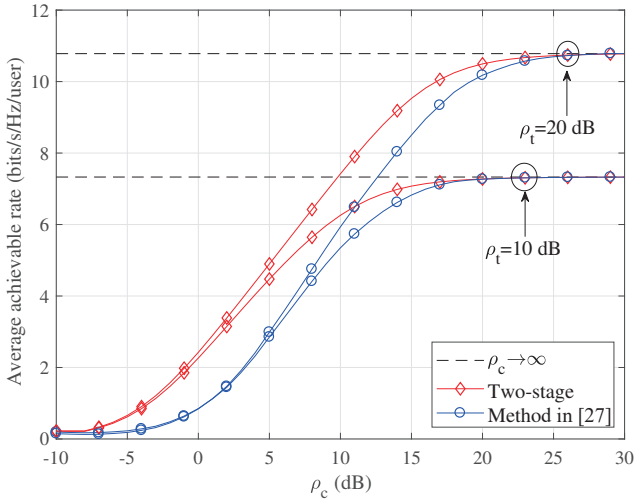

Fig. 6. Average achievable rate after the reciprocity calibration versus the calibration SNR ρ_c. The parameters of the RF gains are $\delta^2 = 0.1$ and $\theta = \pi/6$, while the downlink transmit SNR $\rho_t = 10$ dB and $\rho_t = 20$ dB.

Firstly, we compare the overhead and the computational complexity by numerical results. The overhead and the complexity of hierarchical calibration can be given by 2560 and 33600, respectively. For the proposed two-stage calibration, the signaling overhead and computational complexity are 73 and 6200, respectively. Hence, both the overhead and the computational complexity of the two-stage calibration is less than those of the hierarchical calibration. This implies the proposed two-stage calibration further reduce the overhead and computational complexity of the reciprocity calibration.

To show the performance of the calibration approaches, we define the average achievable rate as $\bar{R} = \frac{1}{K}\sum_{k=1}^{K} R_k$. The average achievable rate after the reciprocity calibration is illustrated in Fig. 6 versus calibration SNR ρ_c with downlink transmit SNR ρ_t being 10 dB and 20 dB. From the illustration, the achievable rates of both the two-stage calibration and the hierarchical calibration increase with the increase in calibra-

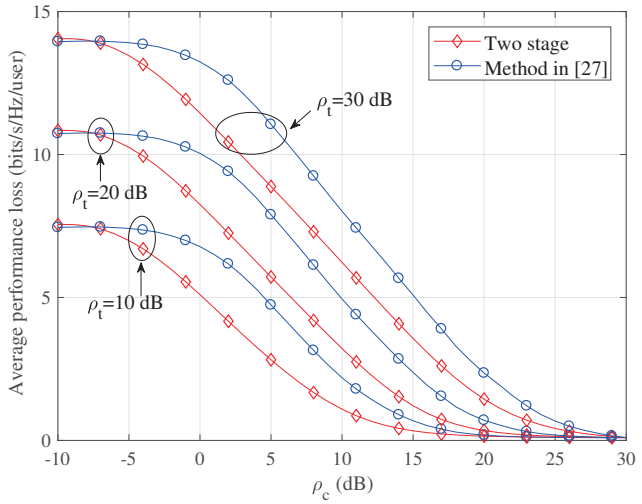

Fig. 7. Average performance loss after the reciprocity calibration versus the calibration SNR ρ_c. The parameters of the RF gains are $\delta^2 = 0.1$ and $\theta = \pi/6$, while the downlink transmit SNR $\rho_t = 10$ dB, $\rho_t = 20$ dB and $\rho_t = 30$ dB.

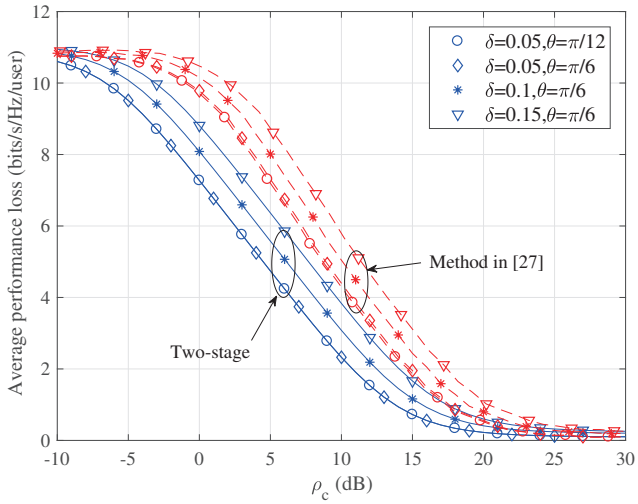

Fig. 8. Average performance loss after the reciprocity calibration versus the calibration SNR ρ_c and mismatch parameters δ^2 and θ. The SNR ρ_t of data transmission is set to 20 dB.

tion SNR. At the low SNR regime, the achievable rate of the two-stage calibration increases faster than that of the hierarchical calibration. And when the achievable rate approaches to the perfection, the two-stage calibration requires lower SNR than the hierarchical calibration. Moreover, compared with the case where the downlink transmit SNR $\rho_t = 10$ dB, the higher SNR case requires lower calibration SNR to achieve the same system performance, which implies that both the downlink transmit SNR and the calibration SNR contribute to the improvement of the system performance. This result is consistent to the theoretical analysis in (29). Also, the proposed two-stage calibration needs lower SNR to achieve the same performance, especially at the lower SNR regime.

Fig. 7 illustrates the average performance loss versus calibration SNR with downlink transmission SNR ρ_c set to 10 dB, 20 dB and 30 dB. As seen from the figure, the performance loss after the reciprocity calibration decreases as calibration SNR ρ_c increases, and it approaches to a lower bound when ρ_c is large. In contrast, when calibration SNR is fixed, the performance loss increases with downlink transmit SNR ρ_t increasing. When the performance loss approaches to the lower bound, the case with $\rho_t = 20$ dB requires higher SNR than the case where $\rho_t = 10$ dB. Similarly, the scenario with $\rho_t = 30$ dB requires higher SNR than the case with $\rho_t = 20$ dB. Hence, consistent with the theoretical results in (30), the system with the higher transmit SNR requires higher calibration SNR to compensate the performance loss caused by the reciprocity mismatch.

The performance loss due to calibration errors is illustrated in Fig. 8 versus difference mismatch parameters with data transmission SNR $\rho_t = 20$ dB. From the figure, it is seen that the performance loss increases with the amplitude mismatch parameter δ^2 increasing, which implies the system with severer hardware imperfection requires more power to compensate the performance loss caused by the hardware imperfection. In contrast, the performance is hardly influenced by the phase

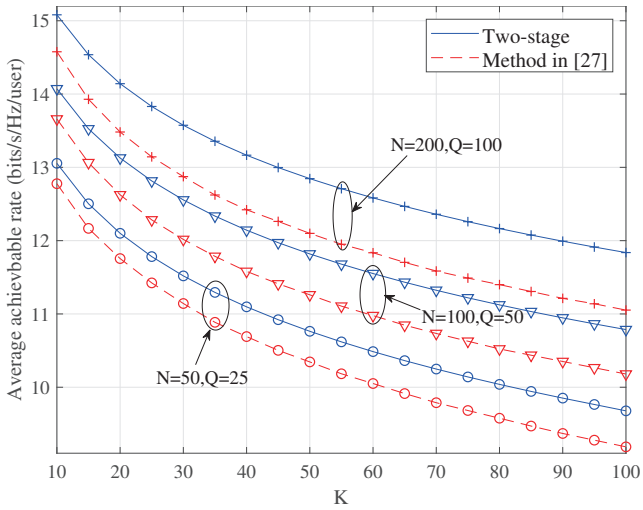

Fig. 9. Average achievable rate with calibration errors versus the number of S-D pairs K. The number of relays is $M = 16$. And the powers of transmission and calibration are set to $\rho_{\rm t} = 20$ dB and $\rho_{\rm d} = 20$ dB respectively.

mismatch parameter θ. This is because the error of imperfect calibration is unrelated to the phase range .

Finally, Fig. 9 demonstrates the average achievable rate after calibration with different number K of S-D pairs and antennas number N of each relay. Both the transmission power $\rho_{\rm t}$ and calibration power $\rho_{\rm d}$ are set to 20 dB. The number Q of antennas of the inter-calibration reference relay is set to $Q = N/2$. From the figure, it is seen that the achievable rate of per S-D pair decreases with the number of S-D pairs increasing and increases with the increase of number of antennas in the relays. And we also find that the performance gap between two-stage calibration and the method in [27] becomes wider when the number of antennas in each relay becomes larger. This is because more antennas can be used to inter-calibration with the increase of antennas of each relay in the proposed two-stage calibration, but the calibration approach in [27] only uses part of antennas in the calibration to avoid large overhead

of the CSI feedback.

VI. Conclusions

In this paper, we have studied the reciprocity mismatch of the relaying system, including the impact analysis and the reciprocity calibration. By considering RF gains as the multiplicative uncertainties in the channel matrix, we have derived the closed-form of the achievable rate with the reciprocity mismatch at first. And the performance losses resulting from the mismatch at the source side, the relay side and the destination side have been investigated as well. The analytical results demonstrated that the mismatch at the relay side severely degrade the system performance, but the mismatch of sources and destinations causes the slight impact. Then, we proposed a two-stage reciprocity calibration approach for the relaying system to calibrate relays. After operating the reciprocity calibration, the closed-form expression of the achievable rate with the estimation errors of calibration coefficients has been derived, and it showed that the imperfect calibration could not cancel IDI completely. Finally, we derived the calibration gain by comparing the performance before and after calibration, which demonstrated that the proposed calibration significantly improved the system performance.

Appendix A
Proof of Proposition 1

A. Derivation of β

By substituting the received signals at relays into the normalization scalar β of the beamforming matrix, the denominator of β is further written as

$$\begin{aligned}\mathbb{E}\left\{\left\|\mathbf{W}_{\mathrm{G}}\mathbf{W}_{\mathrm{H}}\mathbf{x}_{\mathrm{R}}\right\|^2\right\}=\rho_1\mathbb{E}\left\{\left\|\mathbf{W}_{\mathrm{G}}\mathbf{x}_{\mathrm{S}}\right\|^2\right\}+\\ \mathbb{E}\left\{\left\|\mathbf{W}_{\mathrm{G}}\mathbf{W}_{\mathrm{H}}\mathbf{n}_{\mathrm{R}}\right\|^2\right\}.\end{aligned}\tag{33}$$

Then, the addends are derived as follows respectively.

$$\begin{aligned}&\mathbb{E}\left\{\left\|\mathbf{W}_{\mathrm{G}}\mathbf{x}_{\mathrm{S}}\right\|^2\right\}\\ =&\mathbb{E}\left\{\mathrm{tr}\left[(\mathbf{T}_{\mathbf{S}}\mathbf{G}\mathbf{R}\mathbf{R}^*\mathbf{G}^H\mathbf{T}_{\mathbf{S}}^*)^{-1}\right]\right\}\\ =&\mathrm{tr}\left\{(\mathbf{T}_{\mathrm{S}}\mathbf{T}_{\mathrm{S}}^*)^{-1}\mathbb{E}\left[(\mathbf{G}\mathbf{R}\mathbf{R}^*\mathbf{G}^H)^{-1}\right]\right\}.\end{aligned}\tag{34}$$

The distribution of $\mathbf{G}\mathbf{R}\mathbf{R}^*\mathbf{G}^H$ can be approximated as $\mathcal{W}(\frac{1}{MN}\sum_{m=1}^{M}\sum_{n=1}^{N}\mathbf{\Sigma}_{m,n},K,MN)$ [8], where

$$\mathbf{\Sigma}_{m,n}=|r_{m,n}|^2\mathrm{diag}(\phi_{\mathrm{g},m,1},\cdots,\phi_{\mathrm{g},m,K}).\tag{35}$$

Hence, $(\mathbf{G}\mathbf{R}\mathbf{R}^*\mathbf{G}^H)^{-1}$ is inverse Wishart distribution, and (34) can be approximated as

$$\begin{aligned}&\mathbb{E}\left\{\left\|\mathbf{W}_{\mathrm{G}}\mathbf{x}_{\mathrm{S}}\right\|^2\right\}\\ \overset{(a)}{=}&\frac{MN\mathrm{tr}\left\{(\mathbf{T}_{\mathrm{S}}\mathbf{T}_{\mathrm{S}}^*\sum_{m=1}^{M}\sum_{n=1}^{N}\mathbf{\Sigma}_{m,n})^{-1}\right\}}{MN-K}\\ \overset{(b)}{=}&\frac{MN\mathbb{E}\left\{|t_{\mathrm{D},k}|^{-2}\right\}\sum_{k=1}^{K}(\mathrm{tr}\left\{\mathbf{\Phi}_{\mathrm{g},k}\right\})^{-1}}{(MN-K)\mathbb{E}\left\{|r_{m,n}|^2\right\}},\end{aligned}\tag{36}$$

where (a) holds due to $\mathbb{E}\left\{(\mathbf{G}\mathbf{R}\mathbf{R}^*\mathbf{G}^H)^{-1}\right\}\approx\frac{MN(\sum_{m=1}^{M}\sum_{n=1}^{N}\mathbf{\Sigma}_{m,n})^{-1}}{MN-K}$ and (b) is due to Law of Large Numbers (LLN) when MN and K are large [10], [24].

Similarly, the second addend in (33) is approximated as

$$\begin{aligned}&\mathbb{E}\left\{\left\|\mathbf{W}_{\mathrm{G}}\mathbf{W}_{\mathrm{H}}\mathbf{n}_{\mathrm{R}}\right\|^2\right\}\\ \overset{(c)}{=}&\sigma_{\mathrm{rn}}^2\mathrm{tr}\left\{\mathbb{E}\left[(\mathbf{G}_{\mathrm{UL}}^T\mathbf{G}_{\mathrm{UL}}^*)^{-1}\right]\mathbb{E}\left[(\mathbf{H}_{\mathrm{DL}}^T\mathbf{H}_{\mathrm{DL}}^*)^{-1}\right]\right\}\\ \overset{(d)}{=}&\frac{\sum_{k=1}^{K}(|t_{\mathrm{D},k}t_{\mathrm{S},k}|^2\mathrm{tr}\left\{\mathbf{\Phi}_{\mathrm{g},k}\mathbf{R}^*\mathbf{R}\right\}\mathrm{tr}\left\{\mathbf{\Phi}_{\mathrm{h},k}\mathbf{R}^*\mathbf{R}\right\})^{-1}}{(MN-K)^2(MN\sigma_{\mathrm{rn}})^{-2}}\\ \overset{(e)}{=}&\frac{\mathbb{E}\left\{|t_{\mathrm{D},k}t_{\mathrm{S},k}|^{-2}\right\}\sum_{k=1}^{K}(\mathrm{tr}\left\{\mathbf{\Phi}_{\mathrm{g},k}\right\}\mathrm{tr}\left\{\mathbf{\Phi}_{\mathrm{h},k}\right\})^{-1}}{((MN-K)\mathbb{E}\left\{|r_{m,n}|^2\right\})^2(MN\sigma_{\mathrm{rn}})^{-2}},\end{aligned}\tag{37}$$

where (c) is obtained due to the independence between channels $\mathbf{H}_{\mathrm{DL}}$ and channels $\mathbf{G}_{\mathrm{UL}}$, (d) follows (36) since both $(\mathbf{G}\mathbf{R}\mathbf{R}^*\mathbf{G}^H)^{-1}$ and $(\mathbf{H}\mathbf{R}\mathbf{R}^*\mathbf{H}^H)^{-1}$ are inverse Wishart distribution, and (e) is due to LLN.

According to (36) and (37), the following equalities can be obtained as $\mathbb{E}\left\{\left\|\mathbf{W}_{\mathrm{G}}\mathbf{W}_{\mathrm{H}}\mathbf{n}\right\|^2\right\}\ll 1$ and $\mathbb{E}\left\{\left\|\mathbf{W}_{\mathrm{G}}\mathbf{x}_{\mathrm{H}}\right\|^2\right\}\gg\mathbb{E}\left\{\left\|\mathbf{W}_{\mathrm{G}}\mathbf{W}_{\mathrm{H}}\mathbf{n}\right\|^2\right\}$, when MN is much large than K. Hence, compared with $\mathbb{E}\left\{\left\|\mathbf{W}_{\mathrm{G}}\mathbf{x}_{\mathrm{H}}\right\|^2\right\}$, $\mathbb{E}\left\{\left\|\mathbf{W}_{\mathrm{G}}\mathbf{W}_{\mathrm{H}}\mathbf{n}\right\|^2\right\}$ is too small to be ignored. Accordingly, by substituting the (36) into (33), the normalization factor is approximated as

$$\beta\approx\frac{(MN-K)\mathbb{E}\left\{|r_{m,n}|^2\right\}}{\rho_1 MN\sum_{k=1}^{K}(\mathrm{tr}\left\{\mathbf{\Phi}_{\mathrm{g},k}\right\})^{-1}\mathbb{E}\left\{|t_{\mathrm{D},k}|^{-2}\right\}}.\tag{38}$$

B. Derivations of $|b_{k,k}|^2$ and $|b_{k,i}|^2$

By substituting the beamforming matrix $\mathbf{W}$ into the second communication phase, the effective channel $b_{k,i}(i=1,\cdots,K)$ of the k-th destination is denoted as

$$b_{k,i}=\sqrt{\rho_2\beta}\mathbf{g}_{\mathrm{DL},k}[\mathbf{G}_{\mathrm{UL}}^*(\mathbf{G}_{\mathrm{UL}}^T\mathbf{G}_{\mathrm{UL}}^*)^{-1}]_{\cdot i}.\tag{39}$$

When MN is large, $(\mathbf{G}_{\mathrm{UL}}^T\mathbf{G}_{\mathrm{UL}}^*)^{-1}$ can be approximated as a diagonal matrix in the following form [8]

$$\begin{aligned}&\left(\mathbf{G}_{\mathrm{UL}}^T\mathbf{G}_{\mathrm{UL}}^*\right)^{-1}\\ =&\left(\mathbf{T}_{\mathrm{D}}\mathbf{G}^T\mathbf{R}\mathbf{R}^*\mathbf{G}^*\mathbf{T}_{\mathrm{D}}^*\right)^{-1}\\ =&\frac{\mathrm{diag}\left((|t_{\mathrm{D},1}|^2\psi_{2,1})^{-1},\cdots,(|t_{\mathrm{D},K}|^2\psi_{2,K})^{-1}\right)}{MN\mathbb{E}\left\{|r_{m,n}|^2\right\}},\end{aligned}\tag{40}$$

where $\psi_{2,k}=(MN)^{-1}\mathrm{tr}\left\{\mathbf{\Phi}_{\mathrm{g},k}\right\}$.

Then, we have

$$\begin{aligned}|b_{k,k}|^2&=\rho_2|\mathbf{g}_{\mathrm{DL},k}[\mathbf{G}_{\mathrm{UL}}^*(\mathbf{G}_{\mathrm{UL}}^T\mathbf{G}_{\mathrm{UL}}^*)^{-1}]_{\cdot k}|^2\\ &=\frac{\rho_2\beta|r_{\mathrm{D},k}|^2|\mathbf{g}_k\mathbf{T}\mathbf{R}^*\mathbf{g}_k^H|^2}{|t_{\mathrm{D},k}\mathbb{E}\left\{|r_{m,n}|^2\right\}\psi_{2,k}|^2}\\ &\overset{(a)}{=}\frac{\rho_2\beta|\mathbb{E}\left\{t_{m,n}r_{m,n}^*\right\}\psi_{2,k}r_{\mathrm{D},k}|^2}{|\mathbb{E}\left\{|r_{m,n}|^2\right\}\psi_{2,k}t_{\mathrm{D},k}|^2}\\ &\overset{(b)}{\approx}\frac{\rho_2(MN-K)|\mathbb{E}\left\{t_{m,n}r_{m,n}^*\right\}|^2}{\rho_1\mathbb{E}\left\{|r_{m,n}|^2\right\}\psi_1\mathbb{E}\left\{|t_{\mathrm{D},k}|^{-2}\right\}},\end{aligned}\tag{41}$$

where (a) follows because $\mathbf{g}_k\mathbf{T}\mathbf{R}^*\mathbf{g}_k^H$ tends to be $\mathbb{E}\left\{t_{m,n}r_{m,n}^*\right\}\mathrm{tr}\left\{\mathbf{\Phi}_{\mathrm{g},k}\right\}$ when MN is large and (b) holds due to $|t_{\mathrm{D},k}|^2/|r_{\mathrm{D},k}|^2\approx 1$ when the amplitude mismatch is small.

Similarly, $|b_{k,i}|^2 (i \neq k)$ can be given as

$$\begin{aligned}|b_{k,i}|^2 =& \rho_2\beta|\mathbf{g}_{\mathrm{DL},k}[\mathbf{G}_{\mathrm{UL}}^*(\mathbf{G}_{\mathrm{UL}}^T\mathbf{G}_{\mathrm{UL}}^*)^{-1}]_{\cdot i}|^2 \\ \overset{(c)}{=}& \frac{\rho_2\beta|\mathbf{g}_k(\mathbf{T}-\mathbf{R})\mathbf{R}^*\mathbf{g}_i^H|^2(MN)^{-1}}{(\mathbb{E}\{|r_{m,n}|^2\})^2\psi_{2,i}^2|r_{\mathrm{D},k}|^{-2}|t_{\mathrm{D},i}|^2} \\ \overset{(d)}{=}& \frac{\rho_2\beta\mathbb{E}\left\{|t_{m,n}-r_{m,n}|^2\right\}\psi_{3,k,i}|r_{\mathrm{D},k}|^2}{MN\mathbb{E}\{|r_{m,n}|^2\}\psi_{2,i}^2|t_{\mathrm{D},i}|^2} \\ \overset{(e)}{\approx}& \frac{\rho_2(MN-K)\mathbb{E}\left\{|t_{m,n}-r_{m,n}|^2\right\}\psi_{3,k,i}}{\rho_1 MN\psi_1\psi_{2,i}^2\mathbb{E}\{|t_{\mathrm{D},k}|^{-2}\}},\end{aligned} \tag{42}$$

where $\psi_{3,k,i} = (MN)^{-1}\mathrm{tr}\{\mathbf{\Phi}_{\mathrm{g},k}\mathbf{\Phi}_{\mathrm{g},i}\}$, (c) is due to $\mathbf{g}_k\mathbf{T}[\mathbf{R}^*\mathbf{G}^*(\mathbf{G}\mathbf{R}\mathbf{R}^*\mathbf{G})^{-1}]_{\cdot i} = \mathbf{g}_k(\mathbf{T}-\mathbf{R})[\mathbf{R}^*\mathbf{G}^*(\mathbf{G}\mathbf{R}\mathbf{R}^*\mathbf{G})^{-1}]_{\cdot i}$, (d) is obtained due to the independence between $\mathbf{g}_k$ and $\mathbf{g}_i (i \neq k)$ and (e) holds due to $|r_{\mathrm{D},k}|^2/|t_{\mathrm{D},i}|^2 \approx 1$ when the amplitude mismatch is small.

C. Derivation of the Power of Received Noises

By substituting the beamforming matrix $\mathbf{W}$ into (8), $\|\mathbf{g}_{\mathrm{DL},k}\mathbf{W}\|^2$ is further derived as

$$\begin{aligned}&\|\mathbf{g}_{\mathrm{DL},k}\mathbf{W}\|^2 \\ =&\rho_2\beta\left\|\mathbf{g}_{\mathrm{DL},k}\mathbf{W}_{\mathrm{G}}\mathbf{W}_{\mathrm{H}}\right\|^2 \\ =&\rho_2\beta\mathbf{g}_{\mathrm{DL},k}\mathbf{W}_{\mathrm{G}}(\mathbf{H}_{\mathrm{DL}}^H\mathbf{H}_{\mathrm{DL}})^{-1}\mathbf{W}_{\mathrm{G}}^H{\mathbf{g}_{\mathrm{DL},k}}^H \\ \overset{(a)}{=}&\rho_2\beta\frac{\mathbf{g}_{\mathrm{DL},k}\mathbf{W}_{\mathrm{G}}(\mathbf{T}_{\mathrm{S}}\mathbf{T}_{\mathrm{S}}^*)^{-1}\mathbf{W}_{\mathrm{G}}^H{\mathbf{g}_{\mathrm{DL},k}}^H}{\psi_1\psi_{6,k}} \\ \overset{(b)}{=}&\frac{\sum_{i=1}^K|b_{k,i}|^2|t_{\mathrm{S},i}|^{-2}}{(MN-K)\mathbb{E}\{|r_{m,n}|^2\}\psi_{4,k}},\end{aligned} \tag{43}$$

where $\psi_{4,k} = \frac{1}{MN}\mathrm{tr}\{\mathbf{\Phi}_{\mathrm{h},k}\}$, (a) follows because of (35) and the independence between $\mathbf{G}_{\mathrm{DL}}$ and $\mathbf{H}_{\mathrm{DL}}$, and (b) holds according to (38), (40), (41), and (42).

Since the large-scale path loss is always large than 0 and MN is large, $\psi_{2,i}^2 \gg \psi_{3,k,i}$ and $(MN-K)/(MN) \ll MN-K$. Hence, $|b_{k,k}|^2 \gg |b_{k,i}|^2$. Then, it is approximated as

$$\begin{aligned}\|\mathbf{g}_{\mathrm{DL},k}\mathbf{W}\|^2 \approx& \frac{|b_{k,k}|^2|t_{\mathrm{S},k}|^{-2}}{(MN-K)\mathbb{E}\{|r_{m,n}|^2\}\psi_{4,k}} \\ =& \frac{\rho_2|\mathbb{E}\left\{t_{m,n}r_{m,n}^*\right\}|^2|t_{\mathrm{S},k}|^{-2}}{\rho_1\psi_1\psi_{4,k}(\mathbb{E}\{|r_{m,n}|^2\})^2\mathbb{E}\{|t_{\mathrm{D},k}|^{-2}\}}.\end{aligned} \tag{44}$$

D. Achievable Rate

By substituting (41), (42) and (44) into (10), the closed-form of the SINR at the k-th destination can be given as

$$\gamma_k = \frac{\mathit{\Gamma}_k^{\mathrm{ES}}}{\mathit{\Gamma}_k^{\mathrm{IDI}} + \mathit{\Gamma}_k^{\mathrm{rn}} + \mathit{\Gamma}_k^{\mathrm{yn}}}, \tag{45}$$

where

$$\begin{aligned}\mathit{\Gamma}_k^{\mathrm{ES}} &= \frac{(MN-K)|\mathbb{E}\left\{t_{m,n}r_{m,n}^*\right\}|^2}{\mathbb{E}\{|r_{m,n}|^2\}}, \\ \mathit{\Gamma}_k^{\mathrm{IDI}} &= \sum_{i\neq k}^K\frac{(MN-K)\mathbb{E}\left\{|t_{m,n}-r_{m,n}|^2\right\}}{MN\psi_{2,i}^2\psi_{3,k,i}^{-1}}, \\ \mathit{\Gamma}_k^{\mathrm{rn}} &= \frac{|\mathbb{E}\left\{t_{m,n}r_{m,n}^*\right\}|^2\sigma_{\mathrm{rn}}^2}{\rho_1(\mathbb{E}\{|r_{m,n}|^2\})^2\psi_{4,k}|t_{\mathrm{S},k}|^2},\end{aligned} \tag{46}$$

and

$$\mathit{\Gamma}_k^{\mathrm{yn}} = \frac{\sigma_{\mathrm{yn}}^2\psi_1\mathbb{E}\left\{|t_{\mathrm{D},k}|^{-2}\right\}}{\rho_2}. \tag{47}$$

According to $\mathbb{E}\left\{\log\left(1+\frac{1}{x}\right)\right\} \geq \log\left(1+\frac{1}{\mathbb{E}\{x\}}\right)$, a lower bound of the achievable rate at the k-th S-D pair defined in (9) can be given as

$$\begin{aligned}R_k &\geq \log\left(1+\frac{\mathit{\Gamma}_k^{\mathrm{ES}}}{\mathbb{E}\left\{\mathit{\Gamma}_k^{\mathrm{IDI}}+\mathit{\Gamma}_k^{\mathrm{rn}}+\mathit{\Gamma}_k^{\mathrm{yn}}\right\}}\right) \\ &= \log\left(1+\frac{\bar{\mathit{\Gamma}}_k^{\mathrm{ES}}}{\bar{\mathit{\Gamma}}_k^{\mathrm{IDI}}+\bar{\mathit{\Gamma}}_k^{\mathrm{rn}}+\bar{\mathit{\Gamma}}_k^{\mathrm{yn}}}\right),\end{aligned} \tag{48}$$

where $\bar{\mathit{\Gamma}}_k^{\mathrm{ES}} = \mathit{\Gamma}_k^{\mathrm{ES}}$, $\bar{\mathit{\Gamma}}_k^{\mathrm{IDI}} = \mathit{\Gamma}_k^{\mathrm{IDI}}$, $\bar{\mathit{\Gamma}}_k^{\mathrm{yn}} = \mathit{\Gamma}_k^{\mathrm{yn}}$ and

$$\bar{\mathit{\Gamma}}_k^{\mathrm{rn}} = \frac{|\mathbb{E}\left\{t_{m,n}r_{m,n}^*\right\}|^2\mathbb{E}\left\{|t_{\mathrm{S},k}|^{-2}\right\}\sigma_{\mathrm{rn}}^2}{(\mathbb{E}\{|r_{m,n}|^2\})^2\psi_{4,k}\rho_1}. \tag{49}$$

Lastly, by exploiting the statistic properties of RF gains [24], the lower bound of the achievable rate with reciprocity mismatch is denoted in Proposition 1.

Appendix B
Proof of Proposition 2

According to (21), $\mathbf{\Omega}_{\mathrm{DL},m}^{\mathrm{iac}} = \bar{\mathbf{\Omega}}_m - \tilde{\mathbf{Z}}_m^{\mathrm{iac}}$. By substituting $\mathbf{\Omega}_{\mathrm{DL},m}^{\mathrm{iac}}$ into the calibration signal $\mathbf{x}_m(u)(m = 1,\cdots,M-1, u = 1,\cdots,M-1)$, we have

$$\begin{aligned}\mathbf{b}_{\mathrm{r}}^T\mathbf{\Omega}_{\mathrm{UL},m}\mathbf{x}_m(u) &= \frac{1}{\sqrt{\eta}Q}\mathbf{1}_Q^T\hat{\mathbf{F}}_M^{\mathrm{iac}}\mathbf{\Omega}_{\mathrm{UL},m}\mathbf{x}_m(u) \\ &= \frac{c_m}{\sqrt{\eta}Q}\mathbf{1}_Q^T(\bar{\mathbf{\Omega}}_m - \tilde{\mathbf{Z}}_m^{\mathrm{iac}})^T\mathbf{x}_m(u) \\ &= c_m(1-\tau_m)p(m,u),\end{aligned} \tag{50}$$

where $\tau_m = \frac{1}{Q}\mathbf{1}_Q^T(\tilde{\mathbf{Z}}_m^{\mathrm{iac}})^T\mathbf{\Gamma}_m\mathbf{1}_Q$.

Hence, the received signal (22) at the reference can be further denoted as

$$\begin{aligned}S_p(u) &= \sum_{m=1}^{M-1}c_m(1-\tau_m)p(m,u) + \mathbf{b}_{\mathrm{r}}^T\mathbf{z}_{\mathrm{UL}}(u) \\ &= \sum_{m=1}^{M-1}c_m e^{-j\frac{2\pi}{M-1}(u-1)(m-1)} + \tilde{z}(u),\end{aligned} \tag{51}$$

where $\tilde{z}(u) = \mathbf{b}_{\mathrm{r}}^T\mathbf{z}_{\mathrm{UL}}(u) - \sum_{m=1}^{M-1}c_m\tau_m e^{-j\frac{2\pi}{M-1}(u-1)(m-1)}$.

Then, by defining some vectors as $\mathbf{c} = [c_1,\cdots,c_{M-1}]^T$, $\tilde{\mathbf{z}} = [\tilde{z}(1),\cdots,\tilde{z}(M-1)]$, and $\mathbf{s}_p = [S_p(1),\cdots,S_p(M-1)]^T$, the received signals vector is given as

$$\mathbf{s}_p = \mathbf{A}_{M-1}\mathbf{c} + \tilde{\mathbf{z}}, \tag{52}$$

where $\mathbf{A}_{M-1}$ is a $M-1$ by $M-1$ matrix with the entry $[\mathbf{A}_{M-1}]_{m,u} = p(m,u)(m = 1,\cdots,M-1, u = 1,\cdots,M-1)$. According to the approach of solving the matrix equation in [37], the coefficients can be estimated by LS algorithm. Since $\mathbf{A}_{M-1}$ is full rank, the inter-calibration coefficients can be computed by

$$\hat{\mathbf{c}} = \mathbf{A}_{M-1}^{-1}\mathbf{s}_p. \tag{53}$$

It completes the proof of Proposition 2.

APPENDIX C
PROOF OF PROPOSITION 3

A. Property of $\boldsymbol{\Upsilon}$

According to the equivalent channel after intra-calibration in (21), $\tau_m(m=1,\cdots,M-1)$ can be further denoted as $\tau_m = 1-\tau_m^-$ with $\tau_m^- = \frac{1}{Q}\mathbf{1}_Q^T(\boldsymbol{\Omega}_m^{\mathrm{iac}})^T\boldsymbol{\Gamma}_m\mathbf{1}_Q$. Since N is large and $\boldsymbol{\Omega}_m^{\mathrm{iac}}$ is independent with $\tilde{\mathbf{Z}}_m^{\mathrm{iac}}$, τ_m^- can be further denoted as

$$\begin{aligned}\tau_m^- &= \frac{1}{Q}\sum_{q=1}^{Q}\frac{\rho_c\phi_{m,M}|t_{M,q}|^2}{\mathbb{E}\left\{|r_{m,n}|^{-2}\right\}\sigma_z^2+\rho_c\phi_{m,M}|t_{M,q}|^2}\\ &\overset{(a)}{=}\mathbb{E}\left\{\frac{\rho_c\phi_{m,M}|t_{M,q}|^2}{\mathbb{E}\left\{|r_{m,n}|^{-2}\right\}\sigma_z^2+\rho_c\phi_{m,M}|t_{M,q}|^2}\right\}\\ &\overset{(b)}{\geq}\frac{\rho_c\phi_{m,M}}{\mathbb{E}\left\{|r_{m,n}t_{M,q}|^{-2}\right\}\sigma_z^2+\rho_c\phi_{m,M}},\end{aligned} \tag{54}$$

where (a) follows due to LLN and (b) is due to the Jensen's inequality as $\mathbb{E}\{1/(1+x)\} \geq 1/(1+\mathbb{E}\{x\})$. When the amplitude mismatch is small, τ_m can be approximated as

$$\begin{aligned}\tau_m &\approx \frac{\sigma_z^2\mathbb{E}\left\{|r_{m,n}t_{M,q}|^{-2}\right\}}{\sigma_z^2\mathbb{E}\left\{|r_{m,n}t_{M,q}|^{-2}\right\}+\rho_c\phi_{m,M}}\\ &= \frac{\sigma_z^2 e^{2\delta_{\mathrm{r}}^2+2\delta_{\mathrm{t}}^2}}{\sigma_z^2 e^{2\delta_{\mathrm{r}}^2+2\delta_{\mathrm{t}}^2}+\rho_c\phi_{m,M}}.\end{aligned} \tag{55}$$

Hence, when N and Q are large, τ_m tends to be a constant, which is unrelated to c_m.

B. Property of $\tilde{\mathbf{n}} = \mathbf{A}^{-1}\tilde{\mathbf{z}}_{\mathrm{UL}}$

Since entries of $\mathbf{A}_{(U)}$ are constant, the mean of $\tilde{\mathbf{n}}$ can be given as

$$\mathbb{E}\{\tilde{\mathbf{n}}\} = \mathbf{A}^{-1}\mathbb{E}\{\tilde{\mathbf{z}}_{\mathrm{UL}}\} = \mathbf{0}. \tag{56}$$

And the variance of $\tilde{\mathbf{n}}$ can be denoted as

$$\begin{aligned}\mathrm{var}\{\tilde{\mathbf{n}}\} &= \mathbb{E}\left\{\mathbf{A}^{-1}\tilde{\mathbf{z}}_{\mathrm{UL}}\tilde{\mathbf{z}}_{\mathrm{UL}}^H\mathbf{A}^{-H}\right\}\\ &= \frac{|\alpha_M|^2\mathbb{E}\left\{|t_{M,q}r_{M,q}^{-1}|^2\right\}\sigma_z^2}{(M-1)\rho_c Q\varsigma}\mathbf{I}_{M-1}.\end{aligned} \tag{57}$$

When N is large, ς tends to be a constant as

$$\varsigma \overset{(36)}{\approx} \frac{(\mathbb{E}\left\{|t_{m,n}|^2\right\})^2}{(N-Q+1)^{-1}Q}\min_m\{\phi_{M,m}\}. \tag{58}$$

Then, as the mismatch is slight, it is further denoted as

$$\mathrm{var}\{\tilde{\mathbf{n}}\} \approx |\alpha_M|^2\lambda_{\tilde{n}}\mathbf{I}_{M-1}, \tag{59}$$

with

$$\lambda_{\tilde{n}} = \frac{\sigma_z^2 e^{2\delta_{\mathrm{r}}^2-2\delta_{\mathrm{t}}^2}\min_m\{\phi_{M,m}\}}{\rho_c(M-1)(N-Q+1)}. \tag{60}$$

C. Achievable Rate After Calibration

Same as Appendix A, by substituting the equivalent channel $\bar{\mathbf{G}}$ into the beamforming matrix $\mathbf{W}$, $|b_{k,k}^{\mathrm{cal}}|^2$, $|b_{k,i}^{\mathrm{cal}}|^2$ and the power of equivalent noises can be denoted as

$$\begin{aligned}|b_{k,k}^{\mathrm{cal}}|^2 &= \frac{\rho_2(MN-K)\mathbb{E}\left\{|t_{m,n}|^2\right\}|1-\lambda_\tau|^2}{(1+\lambda_{\tau^2}-\lambda_\tau+\mathbb{E}\left\{|\alpha_m|^2\right\}\lambda_{\tilde{n}})\mathbb{E}\left\{|t_{\mathrm{D},k}|^{-2}\right\}\psi_1},\\ |b_{k,i}^{\mathrm{cal}}|^2 &= \sum_{i\neq k}^{K}\frac{\rho_2(MN-K)(\lambda_{\tau^2}+\mathbb{E}\left\{|\alpha_m|^2\right\}\lambda_{\tilde{n}})}{MN(\mathbb{E}\left\{|t_{m,n}|^2\right\}\psi_{3,k,i})^{-1}\mathbb{E}\left\{|t_{\mathrm{D},k}|^{-2}\right\}\psi_1\psi_{2,i}^2},\\ \|\bar{\mathbf{g}}_k\bar{\mathbf{W}}\|^2 &= \frac{\rho_2|1-\lambda_\tau|^2|t_{\mathrm{S},k}|^{-2}(\psi_{4,k}\psi_1)^{-1}}{\rho_1(1+\lambda_{\tau^2}-\lambda_\tau+\mathbb{E}\left\{|\alpha_m|^2\right\}\lambda_{\tilde{n}})\mathbb{E}\left\{|t_{\mathrm{D},k}|^{-2}\right\}}.\end{aligned} \tag{61}$$

where $\lambda_\tau = \frac{1}{M-1}\sum_{m=1}^{M-1}\tau_m$ and $\lambda_{\tau^2} = \frac{1}{M-1}\sum_{m=1}^{M-1}\tau_m^2$.

Then, same as (48), by using the Jansen's equality and exploiting the statistics properties of RF gains, the achievable rate after calibration can be approximated as Proposition 3.

REFERENCES

[1] S. Jin, X. Liang, K. K. Wong, X. Gao, and Q. Zhu, "Ergodic Rate Analysis for Multipair Massive MIMO Two-Way Relay Networks," *IEEE Trans. Wirel. Commun.*, vol. 14, no. 3, pp. 1480–1491, 2015.

[2] Z. Sheng, H. D. Tuan, T. Q. Duong, and H. V. Poor, "Joint Power Allocation and Beamforming for Energy-Efficient Two-Way Multi-Relay Communications," *IEEE Trans. Wirel. Commun.*, vol. 16, no. 10, pp. 6660–6671, 2017.

[3] T. N. Do, D. B. Da Costa, T. Q. Duong, and B. An, "Improving the Performance of Cell-Edge Users in NOMA Systems Using Cooperative Relaying," *IEEE Trans. Commun.*, vol. 66, no. 5, pp. 1883–1901, 2018.

[4] Y. Cai, Y. Xu, Q. Shi, B. Champagne, and L. Hanzo, "Robust joint hybrid transceiver design for millimeter wave full-duplex MIMO relay systems," *IEEE Trans. Wirel. Commun.*, vol. 18, no. 2, pp. 1199–1215, 2019.

[5] S. Gong, C. Xing, S. Ma, Z. Zhang, and Z. Fei, "Secure Wideband Beamforming Design for Two-Way MIMO Relaying Systems," *IEEE Trans. Veh. Technol.*, vol. 68, no. 4, pp. 3472–3486, 2019.

[6] C. D. Ho, H. Q. Ngo, M. Matthaiou, and T. Q. Duong, "On the Performance of Zero-Forcing Processing in Multi-Way Massive MIMO Relay Networks," *IEEE Commun. Lett.*, vol. 21, pp. 849–852, apr 2017.

[7] C. Shan, L. Chen, X. Chen, and W. Wang, "A general matched filter design for reciprocity calibration in multiuser massive MIMO systems," *IEEE Trans. Veh. Technol.*, vol. 67, no. 9, pp. 8939–8943, 2018.

[8] A. Minasian, S. ShahbazPanahi, and R. S. Adve, "Distributed massive MIMO systems with non-reciprocal channels: Impacts and robust beamforming," *IEEE Trans. Commun.*, vol. 66, no. 11, pp. 5261–5277, 2018.

[9] D. Mi, M. Dianati, L. Zhang, S. Muhaidat, and R. Tafazolli, "Massive MIMO Performance With Imperfect Channel Reciprocity and Channel Estimation Error," *IEEE Trans. Commun.*, vol. 65, no. 9, pp. 3734–3749, 2017.

[10] W. Zhang, H. Ren, C. Pan, M. Chen, R. C. De Lamare, B. Du, and J. Dai, "Large-scale antenna systems with UL/DL hardware mismatch: Achievable rates analysis and calibration," *IEEE Trans. Commun.*, vol. 63, no. 4, pp. 1216–1229, 2015.

[11] C. Shan, Y. Zhang, L. Chen, X. Chen, and W. Wang, "Performance Analysis of Large Scale Antenna System with Carrier Frequency Offset, Quasi-Static Mismatch and Channel Estimation Error," *IEEE Access*, vol. 5, pp. 26135–26145, 2017.

[12] H. Wei, D. Wang, J. Wang, and X. You, "Impact of RF mismatches on the performance of massive MIMO systems with ZF precoding," *Sci. China Inf. Sci.*, vol. 59, no. 2, pp. 1–14, 2016.

[13] X. Jiang, M. Cirkic, F. Kaltenberger, E. G. Larsson, L. Deneire, and R. Knopp, "MIMO-TDD reciprocity under hardware imbalances: Experimental results," *IEEE Int. Conf. Commun.*, vol. 2015-Septe, pp. 4949–4953, 2015.

[14] T. Magounaki, F. Kaltenberger, X. Jiang, C. Buey, P. Ratajczak, and F. Ferrero, "Experimental evaluation of relative calibration in a MISO-TDD system," *Eur. Conf. Networks Commun.*, pp. 1–5, 2017.

[15] T. Nishimori, Kentaro and Cho, Keizo and Takatori, Yasushi and Hori, "Automatic calibration method using transmitting signals of an adaptive array for TDD systems," *IEEE Trans. Veh. Technol.*, vol. 50, no. 6, pp. 1636–1640, 2001.

[16] A. Bourdoux, B. Come, and N. Khaled, "Non-reciprocal transceivers in OFDM/SDMA systems: Impact and mitigation," in *Radio and Wireless Conference, 2003. RAWCON'03. Proceedings*, pp. 183–186, IEEE, 2003.

[17] M. Guillaud, D. T. M. Slock, R. Knopp, I. Eur, and S. A. Cedex, "A practical method for wireless channel reciprocity calibration," pp. 1–4.

[18] F. Kaltenberger, J. Haiyong, M. Guillaud, and R. Knopp, "Relative channel reciprocity calibration in MIMO/TDD systems," *Proc. Futur. Netw. Mob. Summit*, pp. 1–10, 2010.

[19] M. Petermann, M. Stefer, D. Wübben, M. Schneider, and K. D. Kammeyer, "Low-complexity calibration of mutually coupled non-reciprocal multi-antenna OFDM transceivers," *Proc. 2010 7th Int. Symp. Wirel. Commun. Syst. ISWCS'10*, no. 1, pp. 285–289, 2010.

[20] B. Kouassi, I. Ghauri, and L. Deneire, "Estimation of Time-Domain Calibration Parameters to Restore MIMO-TDD Channel Reciprocity," *2012 7th Int. ICST Conf. Cogn. Radio Oriented Wirel. Networks Commun.*, pp. 254–258, 2012.

[21] A. Benzin and G. Caire, "Internal self-calibration methods for large scale array transceiver software-defined radios," in *Proc. IEEE Int. ITG Workshop Smart Antennas*, pp. 1–8, VDE, 2017.

[22] R1-092359, "Hardware calibration requirement for dual layer beamforming," Huawei, Los Angeles, CA, USA, 3GPP RAN1 57, Jun. 2009.

[23] C. Shepard, H. Yu, N. Anand, E. Li, T. Marzetta, R. Yang, and L. Zhong, "Argos: practical many-antenna base stations," *Proc. 18th Annu. Int. Conf. Mob. Comput. Netw. - Mobicom '12*, pp. 53–64, 2012.

[24] H. Wei, D. Wang, H. Zhu, J. Wang, S. Sun, and X. You, "Mutual Coupling Calibration for Multiuser Massive MIMO Systems," *IEEE Trans. Wirel. Commun.*, vol. 15, no. 1, pp. 606–619, 2016.

[25] X. Jiang, A. Decurninge, K. Gopala, F. Kaltenberger, M. Guillaud, S. Member, D. Slock, and L. Deneire, "A Framework for Over-the-air Reciprocity Calibration for TDD Massive MIMO Systems," *IEEE Trans. Wirel. Commun.*, vol. PP, no. c, pp. 1–16, 2018.

[26] O. Raeesi, A. Gokceoglu, and M. Valkama, "Estimation and Mitigation of Channel Non-Reciprocity in Massive MIMO," *IEEE Trans. Signal Process.*, vol. 66, no. 10, pp. 2711–2723, 2018.

[27] R. Rogalin, O. Y. Bursalioglu, H. C. Papadopoulos, G. Caire, and A. F. Molisch, "Hardware-impairment compensation for enabling distributed large-scale MIMO," *2013 Inf. Theory Appl. Work. ITA 2013 - Conf. Proc.*, pp. 304–313, 2013.

[28] L. Su, C. Yang, G. Wang, and M. Lei, "Retrieving channel reciprocity for coordinated multi-point transmission with joint processing," *IEEE Trans. Commun.*, vol. 62, no. 5, pp. 1541–1553, 2014.

[29] C. M. Chen, S. Blandino, A. Gaber, C. Desset, A. Bourdoux, L. Van Der Perre, and S. Pollin, "Distributed Massive MIMO: A Diversity Combining Method for TDD Reciprocity Calibration," *2017 IEEE Glob. Commun. Conf. GLOBECOM 2017 - Proc.*, vol. 2018-Janua, pp. 1–7, 2018.

[30] R. Nie, L. Chen, C. Shan, and X. Chen, "A decentralized reciprocity calibration approach for cooperative MIMO," *IEEE Access*, vol. 7, pp. 1560–1569, 2019.

[31] T. V. T. Le and Y. H. Kim, "Power and spectral efficiency of multi-pair massive antenna relaying systems with zero-forcing relay beamforming," *IEEE Commun. Lett.*, vol. 19, no. 2, pp. 243–246, 2015.

[32] F. Mansourkiaie and M. H. Ahmed, "Cooperative routing in wireless networks: A comprehensive survey," *IEEE Commun. Surveys Tuts.*, vol. 17, no. 2, pp. 604–626, 2014.

[33] D. Yang, L.-L. Yang, and L. Hanzo, "DFT-based beamforming weight-vector codebook design for spatially correlated channels in the unitary precoding aided multiuser downlink," in *2010 IEEE International Conference on Communications*, pp. 1–5, IEEE, 2010.

[34] J. Suh, C. Kim, W. Sung, J. So, and S. W. Heo, "Construction of a generalized DFT codebook using channel-adaptive parameters," *IEEE Communications Letters*, vol. 21, no. 1, pp. 196–199, 2016.

[35] L. Chen, N. Zhao, Y. Chen, F. R. Yu, and G. Wei, "Over-the-air Computation for IoT Networks: Computing Multiple Functions with Antenna Arrays," *IEEE Internet Things J.*, vol. 4662, no. c, pp. 1–12, 2018.

[36] J. Li, D. Wang, P. Zhu, J. Wang, and X. You, "Downlink Spectral Efficiency of Distributed Massive MIMO Systems with Linear Beamforming under Pilot Contamination," *IEEE Trans. Veh. Technol.*, vol. 67, no. 2, pp. 1130–1145, 2018.

[37] S. Boyd and L. Vandenberghe, *Convex optimization*. Cambridge university press, 2004.

Rongjiang Nie received the B.S. degree in electronic information science and technology from Southwest Jiaotong University, Chengdu, China, in 2017. He is currently pursuing the Ph.D. degree with the Department of Electronic Engineering and Information Science, University of Science and Technology of China. His research interests include reciprocity calibration and cooperative multiple-input multiple-output.

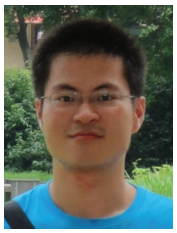

Li Chen received the B.E. in electrical and information engineering from Harbin Institute of Technology, Harbin, China, in 2009 and the Ph.D. degree in electrical engineering from the University of Science and Technology of China, Hefei, China, in 2014. He is currently a faculty member with the Department of Electronic Engineering and Information Science, University of Science and Technology of China. His research interests include wireless IoT communications and wireless optical communications.

Nan Zhao (S'08-M'11-SM'16) is currently a Professor at Dalian University of Technology, China. He received the Ph.D. degree in information and communication engineering in 2011, from Harbin Institute of Technology, Harbin, China.

Dr. Zhao is serving or served on the editorial boards of 7 SCI-indexed journals, including IEEE Transactions on Green Communications and Networking. He won the best paper awards in IEEE VTC 2017 Spring, MLICOM 2017, ICNC 2018, WCSP 2018 and CSPS 2018. He also received the IEEE Communications Society Asia Pacific Board Outstanding Young Researcher Award in 2018.

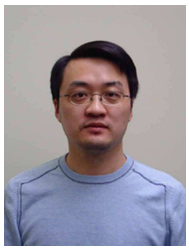

Yunfei Chen (S'02-M'06-SM'10) received his B.E. and M.E. degrees in electronics engineering from Shanghai Jiaotong University, Shanghai, P.R.China, in 1998 and 2001, respectively. He received his Ph.D. degree from the University of Alberta in 2006. He is currently working as an Associate Professor at the University of Warwick, U.K. His research interests include wireless communications, cognitive radios, wireless relaying and energy harvesting.

F. Richard Yu (S'00-M'04-SM'08-F'18) received the PhD degree in electrical engineering from the University of British Columbia (UBC) in 2003. From 2002 to 2006, he was with Ericsson (in Lund, Sweden) and a start-up in California, USA. He joined Carleton University in 2007, where he is currently a Professor. He received the IEEE Outstanding Service Award in 2016, IEEE Outstanding Leadership Award in 2013, Carleton Research Achievement Award in 2012, the Ontario Early Researcher Award (formerly Premiers Research Excellence Award) in 2011, the Excellent Contribution Award at IEEE/IFIP TrustCom 2010, the Leadership Opportunity Fund Award from Canada Foundation of Innovation in 2009 and the Best Paper Awards at IEEE ICNC 2018, VTC 2017 Spring, ICC 2014, Globecom 2012, IEEE/IFIP TrustCom 2009 and Int'l Conference on Networking 2005. His research interests include wireless cyber-physical systems, connected/autonomous vehicles, security, distributed ledger technology, and deep learning.

He serves on the editorial boards of several journals, including Co-Editor-in-Chief for Ad Hoc & Sensor Wireless Networks, Lead Series Editor for IEEE Transactions on Vehicular Technology, IEEE Transactions on Green Communications and Networking, and IEEE Communications Surveys & Tutorials. He has served as the Technical Program Committee (TPC) Co-Chair of numerous conferences. Dr. Yu is a registered Professional Engineer in the province of Ontario, Canada, a Fellow of the Institution of Engineering and Technology (IET), and a Fellow of the IEEE. He is a Distinguished Lecturer, the Vice President (Membership), and an elected member of the Board of Governors (BoG) of the IEEE Vehicular Technology Society.

Guo Wei received the B.S. degree in electronic engineering from the University of Science and Technology of China (USTC), Hefei, China, in 1983 and the M.S. and Ph.D. degrees in electronic engineering from the Chinese Academy of Sciences, Beijing, China, in 1986 and 1991, respectively. He is currently a Professor with the School of information Science and Technology, USTC. His current research interests include wireless and mobile communications, wireless multimedia communications, and wireless information networks.